Global Phosphoproteomics Reveals Crosstalk Between Bcr-Abl and Negative Feedback Mechanisms Controlling Src Signaling

Liudmilla Rubbi, Björn Titz, Lauren Brown, Erica Galvan, Evangelia Komisopoulou, Sharon S. Chen, Tracey Low, Martik Tahmasian, Brian Skaggs, Markus Müschen, Matteo Pellegrini and Thomas G. Graeber (29 March 2011)

Science Signaling **4** (166), ra18. [DOI: 10.1126/scisignal.2001314]

CANCER

Global Phosphoproteomics Reveals Crosstalk Between Bcr-Abl and Negative Feedback Mechanisms Controlling Src Signaling

Liudmilla Rubbi,[1,2,3,4]* Björn Titz,[1,2,3,4]* Lauren Brown,[1,2,3,4] Erica Galvan,[1,2,3,4] Evangelia Komisopoulou,[1,2,3,4] Sharon S. Chen,[1,2,3,4] Tracey Low,[1,2,3,4] Martik Tahmasian,[1,2,3,4] Brian Skaggs,[5] Markus Müschen,[6] Matteo Pellegrini,[7,8] Thomas G. Graeber[1,2,3,4,8]†

In subtypes and late stages of leukemias driven by the tyrosine kinase fusion protein Bcr-Abl, signaling by the Src family kinases (SFKs) critically contributes to the leukemic phenotype. We performed global tyrosine phosphoprofiling by quantitative mass spectrometry of Bcr-Abl–transformed cells in which the activities of the SFKs were perturbed to build a detailed context-dependent network of cancer signaling. Perturbation of the SFKs Lyn and Hck with genetics or inhibitors revealed Bcr-Abl downstream phosphorylation events either mediated by or independent of SFKs. We identified multiple negative feedback mechanisms within the network of signaling events affected by Bcr-Abl and SFKs and found that Bcr-Abl attenuated these inhibitory mechanisms. The C-terminal Src kinase (Csk)–binding protein Pag1 (also known as Cbp) and the tyrosine phosphatase Ptpn18 both mediated negative feedback to SFKs. We observed Bcr-Abl–mediated phosphorylation of the phosphatase Shp2 (Ptpn11), and this may contribute to the suppression of these negative feedback mechanisms to promote Bcr-Abl–activated SFK signaling. Csk and a kinase-deficient Csk mutant both produced similar globally repressive signaling consequences, suggesting a critical role for the adaptor protein function of Csk in its inhibition of Bcr-Abl and SFK signaling. The identified Bcr-Abl–activated SFK regulatory mechanisms are candidates for dysregulation during leukemia progression and acquisition of SFK-mediated drug resistance.

INTRODUCTION

Philadelphia chromosome–positive (Ph+) cases of B cell acute lymphoblastic leukemia (B-ALL) and chronic myelogenous leukemia (CML) are driven by the Bcr-Abl fusion tyrosine kinase. Studies in mouse models have shown that the Src family tyrosine kinases (SFKs) Lyn, Hck, and Fgr are required for the induction of Bcr-Abl–positive B-ALL, but not for the development of CML (*1*). In mouse models of CML, SFKs are implicated in the transition from the initial chronic phase of the disease to the more advanced and aggressive blast crisis stage (*2*).

The tyrosine kinase inhibitor (TKI) dasatinib (Sprycel) causes substantial positive hematological and cytogenetic clinical responses in patients with Ph+ CML or ALL who cannot tolerate or are resistant to the partially selective Abl inhibitor imatinib mesylate (Gleevec) (*3*, *4*). Dasatinib is also more effective than imatinib in controlling mouse models of B-ALL and of CML progression to blast crisis (*2*). Dasatinib has dual specificity against both SFKs and Abl kinases and overall has an intermediate degree of specificity in that it also targets a handful of other kinases (*5*, *6*). In contrast, imatinib is more than 100 times less effective at inhibiting SFKs in comparison to Abl (*6*–*8*). In the context of hematopoietic cells, leukemia, and Bcr-Abl and SFKs, it is noteworthy that dasatinib also inhibits Kit, Tec kinases, and C-terminal Src kinase (Csk). Nonetheless, SFKs are likely some of the most upstream Bcr-Abl–activated, dasatinib-sensitive kinases in leukemia systems. In patient samples, the increased activity of the SFKs Lyn and Hck is associated with resistance to imatinib in cell lines and clinical specimens from patients in late-stage CML (*9*–*13*). Moreover, Lyn silencing induces apoptosis of primary CML blast cells while leaving normal hematopoietic cells unaffected (*14*). Together, these observations point to a critical role for SFKs in subsets of Bcr-Abl–driven pathologies.

SFK function is regulated by tyrosine phosphorylation of critical activation and inhibitory sites, by subcellular localization, by molecular interaction with Src homology 2 (SH2) and SH3 binding proteins, and by ubiquitination and proteasome-mediated degradation (*15*, *16*). SFK catalytic activity is increased by phosphorylation of a tyrosine residue present within the activation loop. This phosphorylation may occur through autophosphorylation and induces a conformational change in the catalytic domain that favors enzymatic activity. Conversely, the phosphorylation of a tyrosine residue located near the C terminus inhibits SFK activity. The final amount of SFK activity is thus the result of the equilibrium between

[1]Crump Institute for Molecular Imaging, David Geffen School of Medicine, University of California, Los Angeles, CA 90095, USA. [2]Institute for Molecular Medicine, David Geffen School of Medicine, University of California, Los Angeles, CA 90095, USA. [3]Jonsson Comprehensive Cancer Center, David Geffen School of Medicine, University of California, Los Angeles, CA 90095, USA. [4]Department of Molecular and Medical Pharmacology, David Geffen School of Medicine, University of California, Los Angeles, CA 90095, USA. [5]Division of Rheumatology, David Geffen School of Medicine, University of California, Los Angeles, CA 90095, USA. [6]Department of Laboratory Medicine, University of California, San Francisco, CA 94143, USA. [7]Institute for Genomics and Proteomics; Department of Molecular, Cell and Developmental Biology, University of California, Los Angeles, CA 90095, USA. [8]California NanoSystems Institute, University of California, Los Angeles, CA 90095, USA.
*These authors contributed equally to this work.
†To whom correspondence should be addressed. E-mail: tgraeber@mednet.ucla.edu

the kinases and the phosphatases that control the phosphorylation status of these two sites.

Many different proteins directly or indirectly regulate SFK activity. Csk phosphorylates the C-terminal tyrosine of SFKs, leading to intramolecular interactions between the site of phosphorylation and the SH2 domains of SFKs, resulting in enzymatic inhibition. Apart from its kinase activity, Csk also interacts through its SH2 and SH3 domains with various proteins, including tyrosine phosphatases and several adaptor proteins. For example, when phosphorylated at specific tyrosine residues, the membrane-bound adaptor Pag1 [phosphoprotein associated with glycosphingolipid microdomains 1, also known as Csk-binding protein (Cbp); hereafter, Pag1] recruits Csk to the plasma membrane, resulting in the inhibition of membrane-localized SFK activity (*17*, *18*). Conversely, the dephosphorylation of the same residues of Pag1, mediated by the tyrosine phosphatase Shp2 (Ptpn11), leads to SFK activation by limiting the recruitment of Csk (*19*). The finding that some Src family members phosphorylate the Csk binding site of Pag1 (*17*, *20*, *21*) suggests the existence of a negative feedback mechanism controlling SFK activity (*22*). The tyrosine phosphatase Ptpn18 (also known as PTP-HSCF), which dephosphorylates the activation domain tyrosine of SFKs, also binds Csk and acts synergistically with Csk to inhibit signaling events triggered by SFKs (*23*).

Here, we investigated the role of SFKs in Ph+ leukemias by providing a system-wide characterization of SFK-related tyrosine phosphorylation events in a Bcr-Abl–driven leukemia cell line model. By perturbing the signaling network at the SFK nodes through pharmacological inhibition or genetic manipulation and measuring the proteome-wide changes in tyrosine phosphorylation by quantitative mass spectrometry (MS), we delineated Bcr-Abl and SFK substrates and constructed a context-dependent model of the feedback mechanisms controlling SFK activity. The most responsive events to SFK perturbation included phosphorylation of proteins associated with three SFK negative feedback mechanisms. Nonetheless, activation from Bcr-Abl appeared to overpower this feedback to promote SFK signaling. Indeed, we also observed the Bcr-Abl–mediated phosphorylation of the phosphatase Shp2, and this phosphorylation may contribute to the repression of SFK negative feedback through Shp2-mediated dephosphorylation of Pag1 (*19*). Finally, perturbation of the SFK negative regulator Csk revealed global network effects on phosphorylation. We found similar global repression, using either wild-type or kinase-deficient Csk, implicating the adaptor protein role of Csk over its inhibitory kinase function.

RESULTS

Network bifurcation revealed by differential dose-response sensitivities

Our approach for investigating network-wide SFK-dependent phosphorylation response patterns in Bcr-Abl–positive cells involved three steps (fig. S1). We perturbed the network (i) with the TKI dasatinib that inhibits the kinase activity of Bcr-Abl mutants and SFKs with differing specificities, (ii) by stable overexpression of SFKs, or (iii) by stable overexpression of wild-type or kinase-deficient SFK regulators. Next, we measured the changes induced by these perturbations with a quantitative MS-based phosphoproteomic assay (*24*–*26*). Finally, we analyzed the phosphorylation events with bioinformatic techniques that incorporate interactions and motifs reported in literature-based protein function and interaction databases. Through the combination of phosphoprofiling and literature-guided analysis, we identified specific subnetworks involved in SFK feedback regulation in the context of Bcr-Abl–driven signaling.

There are many examples of point mutations in the Abl kinase domain that give rise to clinical resistance to Bcr-Abl inhibitors (*27*, *28*). We analyzed murine pro-B, lymphoid, Ba/F3 cells transformed with either the T315A or the T315I mutant of Bcr-Abl, which exhibit differential sensitivities to dasatinib, allowing the effect of dasatinib on Bcr-Abl to be distinguished from its effect on SFKs (Fig. 1A). The Ba/F3 lymphoid system provides a model for Bcr-Abl–positive leukemias in general, including the clinically challenging subset of Bcr-Abl–positive lymphoid B-ALL (*3*, *12*, *29*, *30*). The T315A Bcr-Abl mutant is 100 times more resistant to dasatinib inhibition than are the SFKs [T315A Bcr-Abl IC_{50} (median inhibitory concentration) for growth inhibition, 125 nM; wild-type Bcr-Abl IC_{50}, 1.3 nM (*27*); binding constant (K_d), 0.5 nM (*5*, *6*); SFK K_d, 0.2 to 0.8 nM (*5*, *6*)], and the T315I mutant is 1000-fold more resistant to dasatinib inhibition than is unmutated Bcr-Abl [T315I K_d, 590 nM (*6*); IC_{50} for growth inhibition >1000 nM (*28*)]. The T315A mutation results in a loss of fitness in the absence of drug and confers a milder resistance to dasatinib than that conferred by the T315I mutant, which in the absence of drug is a gain-of-fitness mutation (*24*, *31*).

We performed dose-escalation experiments with Ba/F3 cells transformed with the Bcr-Abl T315A variant. Each sample was treated for 2 hours with defined concentrations of dasatinib. After cell lysis and trypsin digestion of the total proteins, tyrosine-phosphorylated peptides were specifically enriched with pan-specific antibodies that recognize peptides containing phosphorylated tyrosines (anti-phosphotyrosine antibodies) (*25*, *32*). Detection, identification, and quantitation of the phosphopeptides were subsequently performed by liquid chromatography–tandem MS (LC-MS/MS) (see Materials and Methods). Unsupervised hierarchical clustering of the amount of tyrosine phosphorylation identified three groups of events with different dose-response sensitivities (Fig. 1B and fig. S2). The most sensitive group, with a median effective concentration (EC_{50}) estimated at 0.3 nM, likely includes phosphorylation events downstream of SFKs. The events in the most resistant group are likely phosphorylated independently of SFKs because their estimated EC_{50} (50 nM) is close to the previously reported EC_{50} of T315A Bcr-Abl (125 nM) (*28*). The events in the intermediate group (EC_{50} ~9 nM) are likely regulated in a more complex manner, for example, by both Bcr-Abl and SFKs, by a different dasatinib-sensitive kinase, or by a combination of several dasatinib-sensitive kinases. The intermediate specificity of dasatinib raises some potential ambiguity in the interpretation of these results, such as effects from inhibiting Csk, which has a K_d of 1 nM for dasatinib (*5*, *6*). A small cluster of phosphorylation events that initially increased and then decreased with dose escalation was also observed. This bell-shaped dose response may represent targets of the convergence of more than one upstream regulatory pathway with differential dasatinib sensitivities. For example, SFK activity may indirectly impede phosphorylation of these substrates, whereas Bcr-Abl may promote their phosphorylation. We also observed a group of events that increased in phosphorylation upon dasatinib dose escalation, potentially due to release of Bcr-Abl–mediated repression. Control experiments with wild-type Bcr-Abl (p210) treated with dasatinib (fig. S3) demonstrated that, at doses expected to inhibit the respective Bcr-Abl isoforms, the fold change responses of phosphorylation events within the signaling network to drug inhibition were similar irrespective of the isoform driving the signaling (correlation coefficient $R = 0.85$; fig. S3D).

To statistically validate our interpretation that the most dasatinib-sensitive tyrosine phosphorylation events are direct SFK targets or otherwise downstream of SFKs, we asked whether the associated proteins were enriched for SFK-interacting partners or SFK substrates. As an unbiased literature-based reference, we used the curated Human Protein Reference Database (HPRD) (*33*), which includes enzyme-substrate interactions as

well as other physical and functional interactions. Ranking proteins by the average sensitivity of their detected phosphosites to dasatinib, we found that the top of this sensitivity list was significantly enriched for proteins that interact with or are substrates of SFKs (Fig. 1C). We calculated sensitivity scores as the sum of log fold changes induced by the low doses (5 and 25 nM) of dasatinib (see Materials and Methods). We found similar results with the dasatinib-resistant Bcr-Abl variant, T315I (table S1; see table S3 for the complete T315A and T315I data). The statistically significant enrichment signal supports our inference that the most dasatinib-sensitive tyrosine phosphorylation

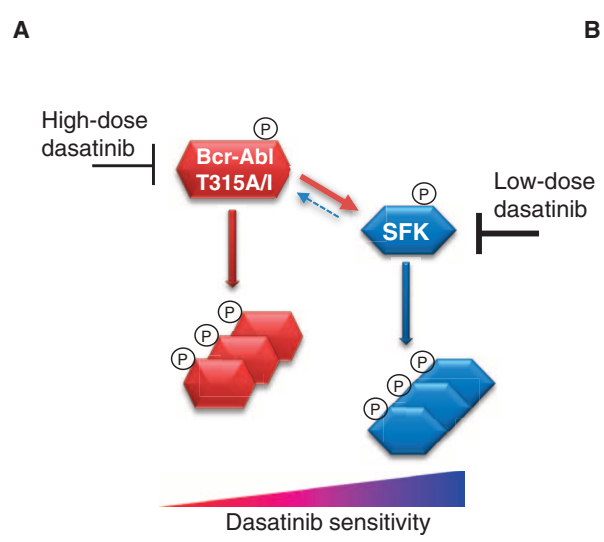

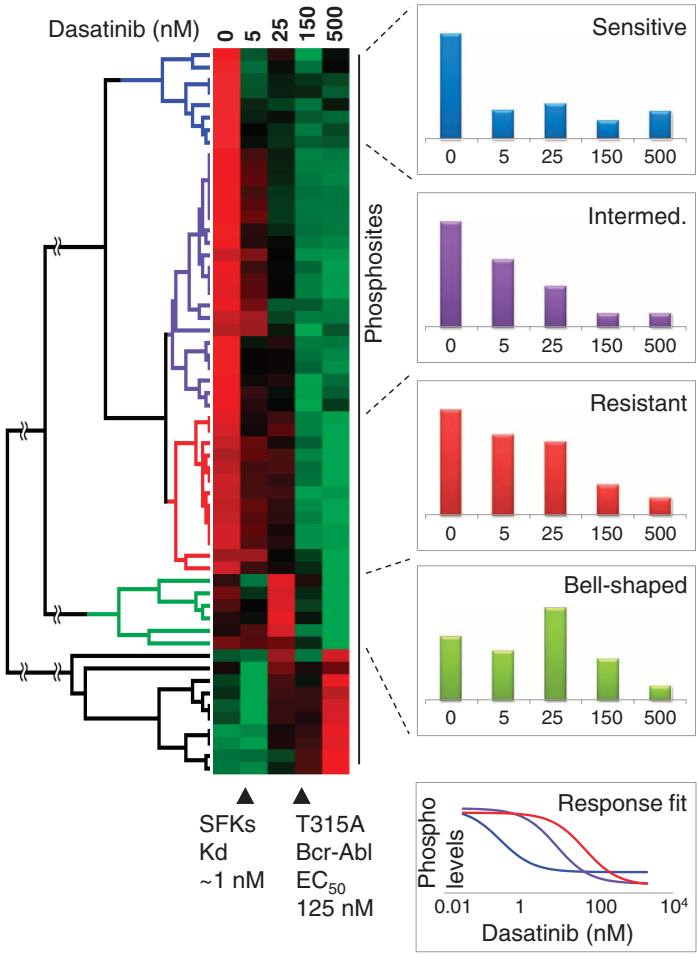

C

Entrez	Phosphopeptide sequence	Phospho site	Sensitivity score	SFK interaction†
Was	LIpYDFIEDQGGLEAVR	Y^{293}	12.6	Substrate/PPI
Btk	VVALpYDYMPMNANDLQLR	Y^{222}	10.3	Substrate/PPI
	VVALYDpYMPMNANDLQLR	Y^{224}		
Hsp90aa1	LVTSPCCIVTSTpY GWTANMER	Y^{604}	7.9	PPI
Pxn	AGEEEHVpYSFPNK	Y^{118}	7.2	PPI
Dapp1	EVEEPCIpYESVR	Y^{139}	7.1	Substrate/PPI
Eif3s6ip	GDPQVYEELFSpYACPK	Y^{415}	7.0	
Prkcd	KLDTTESVGIpYQGFEK	Y^{311}	6.9	Substrate/PPI
Dbi	TQPTDEEMLFIpYSHFK	Y^{28}	6.8	
Csk	VMEGTVAAQDEFpYR	Y^{184}	6.4	PPI

†PPI, SFK-interacting protein enrichment, $P < 0.01$; Substrate, SFK substrate enrichment; $P < 0.01$

Fig. 1. Kinase inhibitor dose-escalation experiments distinguish different arms of the Bcr-Abl signaling network. (**A**) Dasatinib-resistant mutants of Bcr-Abl (T315A, T315I) distinguish Bcr-Abl–initiated phosphorylation events downstream of SFKs from those that are independent of SFKs. SFK-mediated events (blue) would be inhibited by low doses of dasatinib, whereas SFK-independent events (red) would be inhibited by a higher dose of dasatinib. (**B**) Unsupervised hierarchical clustering of dose-response patterns of phosphorylation events from global, label-free quantitative phosphorylation profiling of dasatinib dose-escalation experiments reveals five main clusters identified by color: sensitive to inhibition (blue, EC_{50} 0.3 nM); intermediate sensitivity (intermed.) to inhibition (purple, EC_{50} 9 nM); resistant to inhibition (red, EC_{50} 50 nM); bell-shaped with a peak of activity at moderate concentrations of dasatinib (green); phosphorylation events that increased in the presence of dasatinib (black). The heat map shows relative quantitative amounts (red, high; green, low) of different phosphorylation events (rows) upon treatment of Bcr-Abl–T315A–expressing Ba/F3 cell with escalating dasatinib doses (columns). Results were filtered for events with substantial change (coefficient of variation >0.3) and reproducibility between two replicate experiments (correlation coefficient >0.5). The protein and phosphorylation residue identities are listed in fig. S2. EC_{50} values were calculated for the three decay clusters to a logistic dose-response equation, $1/(1 + [\text{inhibitor}]/EC_{50})$. (**C**) The top-ranked SFK candidate protein substrates determined by ranking of the data shown in (B) to their sensitivity to dasatinib (average sensitivity score of all observed phosphorylation sites on the protein; see Materials and Methods). Protein-protein functional interactions (PPI) with SFKs are based on the HPRD database, and SFK substrates are a subset of the SFK PPI set in HPRD. For each protein, the observed phosphopeptide sequences are listed along with the mouse phosphorylation site residue number. See table S3 for the complete dasatinib sensitivity–ranked T315A and T315I results.

events of the dose-escalation experiments occurred on known or candidate SFK interactors and substrates.

SFK-responsive phosphorylation events defined by kinase perturbation

To further expand and characterize the collection of SFK-related phosphorylation events, we genetically perturbed the SFK network by stable overexpression of the SFKs Lyn or Hck in Bcr-Abl (p210 isoform)–transformed Ba/F3 cells. Lyn and Hck are found primarily in hematopoietic cells, and increased abundance and activation of both these kinases has been found in leukemic blasts from imatinib-resistant CML patients (*9*, *10*). Lyn is present in lymphoid and myeloid cells, whereas Hck is mainly in cells of the myeloid lineage (*16*).

We generated multiple independent cell lines with varying degrees of Lyn and Hck overexpression (Fig. 2). The global changes in tyrosine phosphorylation were identified and quantified by phosphoproteomic MS (left heat map, Fig. 3A). Upon Lyn and Hck overexpression, the amount of tyrosine phosphorylation of many phosphosites was substantially increased. We also observed a smaller number of phosphosites that exhibited decreased tyrosine phosphorylation upon SFK overexpression. Combining the results obtained by the overexpression of Lyn and Hck in Bcr-Abl–transformed cells with those obtained by several independent dasatinib dose-escalation experiments using the Bcr-Abl dasatinib-resistant mutants T315A and T315I (right heat map, Fig. 3A) allowed us to measure 484 unique tyrosine phosphorylation sites (table S3).

As expected, many of the tyrosine phosphorylation events induced by SFK overexpression were repressed by drug inhibition, and vice versa. Accordingly, we assigned an "SFK perturbation response score" to each of these tyrosine phosphorylation events by summing the log of the fold change in the SFK activation experiments (SFK overexpression) and subtracting the sum of the log fold change in the low-dose samples of the SFK drug inhibition experiments and ranked the phosphorylation events by this perturbation response score (Fig. 3A). We expect that a substantial number of the tyrosine phosphorylation events that correlate with SFK activity changes may be direct SFK substrates. In contrast, the tyrosine phosphorylation of sites with negative scores exhibited increased phosphorylation with inhibition of SFK activation and vice versa; they were anticorrelated with SFK activity. We expect that this subset of tyrosine phosphorylation sites is regulated indirectly by SFKs.

To validate our interpretation of the ranked phosphorylation sites, we used statistical enrichment approaches to compare our results with the literature through bioinformatic analyses. The observed phosphorylation sites were evaluated with their SFK perturbation response scores from all experiments combined, as well as with the scores based on overexpression and drug inhibition independently (Fig. 3B and table S1). We found the ranked lists to be statistically enriched for (i) the presence of an Src motif in the phosphorylation site [based on the Scansite database (*34*)], (ii) functional interactions with SFKs [based on HPRD kinase-substrate and protein-protein interactions (PPIs)], and (iii) the presence of an SH2 domain [based on the InterPro database (*35*)] (table S1).

The presence of an Src motif was maximally enriched among the top 316 phosphorylation sites with the highest positive SFK perturbation response scores, indicating that this motif is widespread and only depleted among the group of sites with negative perturbation response scores found at the bottom of our list (Fig. 3, A and B, and table S1). Ranking proteins by the average SFK perturbation response score of their detected phosphosites, we found that the top of this ranked list was significantly enriched for proteins that interacted with or are substrates of SFKs (Fig. 3B and table S1). Six of the top-scoring seven proteins are known SFK interactors (Was, Ptpn18, Fyb, Dapp1, Prkcd, and Pxn), four of which are also known SFK substrates (Was, Fyb, Dapp1, and Prkcd). When the same enrichment analysis was done with the Abl motif and Abl PPIs rather than those for SFKs, the degree of enrichment was not statistically significant (fig. S4). Thus, our experimental design of drug and genetic perturbations targeted at SFKs preferentially enriches for SFK-related motifs, interactors, and substrates in comparison to the Abl-related versions of these properties.

We next defined the consensus sequence motifs of the top 50 phosphorylation sites that had positive SFK perturbation scores and of the 50 phosphorylation sites with SFK perturbation response scores closest to zero (correlated and unchanging phosphosites, respectively) (Fig. 3C). Consistent with the Scansite-based enrichment analysis, the top 50 correlated phosphorylation sites had an in vivo–determined SFK perturbation consensus motif (E/V-E/D-x-L/I-Y-E/D) similar to previously reported in vitro–determined Src motifs: (D)-E-E-I/V-Y-G/E-x-F (c-Src) and (E/D)-E/D-E/D-I/V-Y-G/E/(D)-E-F-D/E (v-Src) (*36*). All three of these motifs have glutamic and aspartic acid residues in positions −3 to −4 and +1 with respect to the tyrosine (Y) residue (Fig. 3C). In contrast, we did not find a notable similarity to the known Src motif when we generated a consensus motif from the 50 phosphosites with scores closest to zero (Fig. 3C). Previous studies have also established that Abl substrates tend to have a conserved proline at the +3 position (*36*). We find that this proline

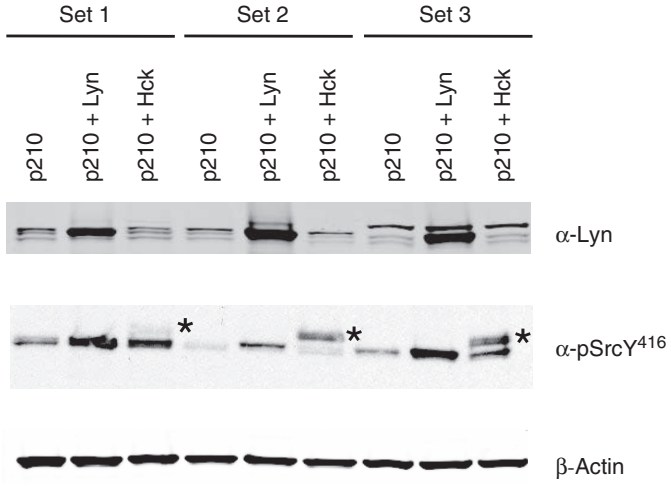

Fig. 2. Stable overexpression of Lyn and Hck in Ba/F3 Bcr-Abl (p210) cells. Ba/F3 Bcr-Abl (p210) cells stably overexpressing human Lyn or Hck were generated by retroviral infections (see Materials and Methods). Representative immunoblot-based abundance of total and phosphorylated Lyn and Hck in the three independently derived sets of cell lines. β-Actin staining confirms equal protein loading on the same membrane. Overexpression of Hck results in the appearance of an additional band of higher molecular weight (indicated by the asterisk) when probing with antibodies against Y^{416}-phosphorylated Src. These antibodies recognize many SFKs due to homology within the family around the activation site, and thus, this additional band is likely phosphorylated Hck. The abundance of Lyn and Hck and their phosphorylated activation site forms are qualitatively higher in sets 2 and 3. An invariant cross-reactive band of unknown origin is seen in the third set of cell lines when probed with the antibody that recognizes Lyn. Expression of exogenous human Hck was also verified by the detection of human-specific phosphorylated Hck peptides by MS (table S3).

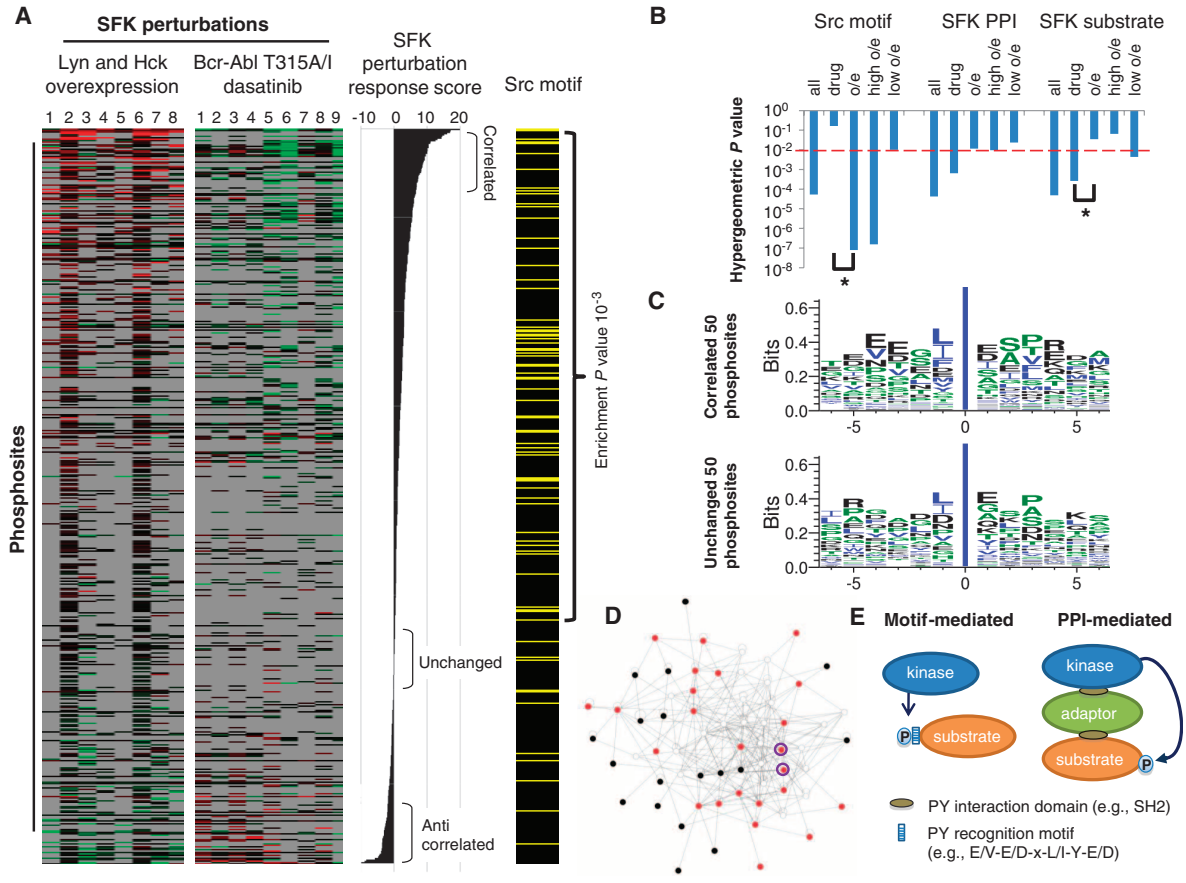

Fig. 3. SFK perturbation response analysis of phosphorylation events identifies subgroups enriched for SFK substrates, interacting proteins, and motifs. (**A**) Ranking phosphorylation events (phosphosites) by their degree and direction of response to genetic and inhibitor-based perturbation of SFKs results in enrichment of phosphorylation sites with canonical Src substrate motifs. The heat maps show 512 phosphorylation events (rows) and their responses to the indicated perturbations. Left heat map columns 1 to 4, p210 + Lyn (samples 1, 2, 2′, 3); columns 5 to 8, p210 + Hck (1, 2, 2′, 3). Right heat map: columns 1 to 3, Bcr-Abl T315A dasatinib 5 nM (1, 2, 3); columns 4 and 5, Bcr-Abl T315A dasatinib 25 nM (1, 2); columns 6 and 7, Bcr-Abl T315I dasatinib 5 nM (1, 2); columns 8 and 9, Bcr-Abl T315I dasatinib 25 nM (1, 2). Lyn and Hck independently derived cell lines are as defined in Fig. 2. Numbers in parentheses indicate independently derived or treated samples. Separately prepared replicates are indicated by a prime. Responses are shown as log fold change values of perturbed over control (red, positive log ratios; green, negative log ratios; gray, not measured). The phosphorylation events were ranked by the sum of their log ratios across overexpression conditions minus the sum of their log ratios across drug conditions (SFK perturbation response score) of the phosphosite. The incidence of a canonical "Src Kinase" motif among these phosphosites is also shown (yellow lines in ladder graph; based on the Scansite resource). The top 316 ranked phosphosites (bracket) are significantly enriched for Src motifs compared to the whole list, with a hypergeometric distribution–based permutation *P* value of 10^{-3} (see Materials and Methods). (**B**) SFK drug inhibition and overexpression perturbation approaches differentially enrich for SFK-related properties (SFK motifs, PPIs, and substrates). Plot shows the likelihood of the observed enrichment of phosphosites or proteins with the indicated SFK-related property at the top of our SFK perturbation response score-ranked lists. Enrichment analysis was performed after ranking phosphosite lists (in the case of motif properties) or protein lists (for the protein-based properties of interactions and substrates) by their perturbation scores with either both the drug- and overexpression-based perturbation experiments or subsets of experiments as indicated. The presence of Src motifs was determined with Scansite; PPIs and kinase substrates were defined by HPRD (substrates are a subset of PPIs). The red dotted line indicates the approximate point (0.01) where the hypergeometric distribution results yield a permutation analysis–based *P* value of 0.05. The asterisks indicate significant differences between drug- and overexpression-based enrichment from permutation analysis ($P_{Permutation} < 0.05$; table S1; see Materials and Methods). o/e, overexpression; high o/e, qualitative high-overexpressing cell lines (sets 2 and 3); low o/e, low-overexpressing cell lines (set 1) (based on the immunoblots in Fig. 2). (**C**) The consensus sequence motifs of the top 50 correlated phosphosites and the 50 with SFK response scores closest to zero (unchanging) show that the correlated sites are enriched for the residue patterns previously associated with Src substrates (*36*). The tyrosine (Y) residue at position zero extends beyond the charted range. (**D**) The network of PPIs between the 40 proteins associated with the top-ranked SFK perturbation-correlated phosphosites (red nodes) and the 40 proteins with the smallest change in response to SFK perturbation (black). The white nodes indicate proteins added by the Ingenuity Pathway Analysis algorithm to complete the network with a maximal number of red ($n = 24$) and black ($n = 18$) input proteins. SFKs are noted by a purple circle surrounding the nodes. This network annotated with protein names is in fig. S5. (**E**) Proposed model of motif- and PPI-mediated substrate recognition mechanisms underlying the differential enrichment trends for SFK overexpression and drug inhibition–based perturbations, respectively.

is equally present in both the correlated and the unchanged phosphosites in the list. Thus, whereas the top of our SFK perturbation response list is enriched for Src substrates, Abl substrates are more evenly distributed throughout the list.

We used the Ingenuity Pathway Analysis software to characterize and visualize the degree of PPIs between the proteins containing the correlated and unchanging phosphosites and created a network for the top 40 correlated and 40 most unchanged proteins (Fig. 3D and fig. S5). This analysis revealed that the correlated proteins (shown in red) interacted among themselves to form a highly connected network that included and made dense links with the SFKs (circled in purple in Fig. 3D). In contrast, the unchanged proteins (shown in black) had fewer interactions.

Overall, the motif and PPI analyses support our interpretation that the phosphorylation sites most responsive to SFK perturbation tend to be functionally connected to SFKs. Many of the positively scoring "SFK-responsive" phosphopeptides in our complete results were not listed in HPRD as SFK substrates or interactors (Table 1 and table S3). Thus, the SFK perturbation list provides many new candidate SFK-linked phosphorylation events.

Overlap and biases in the network response patterns from SFK inhibition or overexpression

To test for differences in the response of the signaling network to distinct perturbations, we applied the SFK interaction and motif enrichment

Table 1. Top-ranked SFK candidate protein substrates and secondary targets based on correlated response to perturbations of SFK activity. Observed phosphorylation events are ranked using the SFK perturbation response scores from Fig. 3A, and the top-ranked events are listed along with their mouse (and human in parentheses) phosphosite residue number. For each protein, only the top-scoring phosphopeptide sequence is listed. The complete results along with fold change values for all drug inhibition and kinase overexpression experiments can be found in table S3. Abbreviations for the amino acids are as follows: A, Ala; C, Cys; D, Asp; E, Glu; F, Phe; G, Gly; H, His; I, Ile; K, Lys; L, Leu; M, Met; N, Asn; P, Pro; Q, Gln; R, Arg; S, Ser; T, Thr; V, Val; W, Trp; and Y, Tyr.

Protein*	Phosphopeptide sequence	Phosphosite	Protein description	SFK perturbation score	Estimated *P* value†	SFK interaction‡
Was	LIpYDFIEDQGGLEAVR	Y^{293} (Y^{290})	Wiskott-Aldrich syndrome	25.8	9.9×10^{-9} (4.8×10^{-6})	Substrate/ PPI
Ptpn18	APTSTDTPIpYSQVAPR	Y^{381} (Y^{389})	Protein tyrosine phosphatase, nonreceptor type 18	17.2	3.0×10^{-5} (1.5×10^{-3})	PPI
Fyb	TTAVEIDpYDSLKR	Y^{560} (Y^{571})	FYN binding protein	17.0	2.3×10^{-7} (3.7×10^{-5})	Substrate/ PPI
Lyn	EEPIpYIITEYMAK	(Y^{316})§	Lyn (Src family kinase)	16.2	1.5×10^{-7} (3.5×10^{-5})	
Lyn	EEPIpYIITEFMAK	Y^{316} (Y^{316})	Lyn (Src family kinase)	15.2	1.0×10^{-6} (1.2×10^{-4})	
Hck	TLDNGGFpYISPR	(Y^{187})§	Hemopoietic cell kinase	14.7	2.0×10^{-6} (1.6×10^{-4})	
Btk	KVVALYDpYMPMNANDLQLR	Y^{224} (Y^{224})	Bruton agammaglobulinemia tyrosine kinase	14.4	1.7×10^{-5} (1.0×10^{-3})	Substrate/ PPI
Pag1	AADTELGPGVEGPpYEVLK	Y^{165} (Y^{163})	Phosphoprotein associated with glycosphingolipid microdomains 1	13.3	1.9×10^{-6} (1.9×10^{-4})	PPI
Dapp1	EVEEPCIpYESVR	Y^{139} (Y^{139})	Dual adaptor of phosphotyrosine and 3-phosphoinositides	11.2	3.8×10^{-5} (1.5×10^{-3})	Substrate/ PPI
Itsn2	GEPEALpYAAVTK	Y^{922} (Y^{941})	Intersectin 2	11.1	3.0×10^{-3} (3.9×10^{-2})	
Hsp90ab1	LVSSPCCIVTSTpYGWTANMER	Y^{596} (Y^{596})	Heat shock protein 90 kD alpha, class B, member 1	10.5	1.4×10^{-2} (9.4×10^{-2})	
Eno1	GNPTVEVDLpYTAK	Y^{24} (F^{25})	Enolase 1 (alpha)	10.5	2.5×10^{-3} (3.7×10^{-2})	
Cbl	VTQEQpYELYCEMGSTFQLCK	Y^{366} (Y^{368})	Cas-Br-M (murine) Ecotropic retroviral transforming sequence	10.5	1.7×10^{-3} (3.2×10^{-2})	Substrate/ PPI
Prkcd	KLDTTESVGIpYQGFEK	Y^{311} (Y^{313})	Protein kinase C, delta	10.3	1.9×10^{-3} (3.3×10^{-2})	Substrate/ PPI
Sgk269	VPIVINPNAYDNLAIpYK	Y^{638} (Y^{641})	NKF3 kinase family member	10.2	1.5×10^{-3} (3.0×10^{-2})	
Actn1	AIMTYVSSFpYHAFSGAQK	Y^{246} (Y^{246})	Actinin, alpha 1	10.1	9.4×10^{-3} (7.2×10^{-2})	
Dok2	SGSPCMEENELpYSSSTTGLCK	Y^{142} (Y^{139})	Docking protein 2	10.0	7.6×10^{-3} (6.3×10^{-2})	PPI
Pxn	AGEEEHVpYSFPNK	Y^{118} (Y^{118})	Paxillin	9.6	5.3×10^{-4} (1.4×10^{-2})	PPI

*Proteins indicated in bold are involved in SFK feedback mechanisms (Fig. 4). †Estimated *P* values for the observed fold changes used to calculate the perturbation score are based on the like sample distributions in fig. S12. Values in parenthesis are Benjamini and Hochberg multiple hypothesis corrected. ‡The SFK interaction column indicates experimental evidence for SFK substrates and SFK protein-protein functional interactions (PPI) based on the HPRD database and is the basis for the enrichment analysis of Figs. 1C and 3B and table S1. In the HPRD database, SFK substrates are a subset of the SFK PPI set. §The human-specific phosphopeptides come from the exogenous expression of Lyn and Hck.

analysis to the overexpression or drug inhibition experiments separately. For the Src motif results, the perturbation response score contributions from the overexpression experiments were primarily responsible for the observed enrichment, because phosphorylation sites ranked by drug response scores were not significantly enriched (Fig. 3B and table S1). Furthermore, the ranking of phosphorylation sites on the basis of experiments in which we achieved qualitatively higher levels of overexpression of Lyn and Hck generated the most significant enrichment for SFK motifs (Fig. 3B). Consensus motifs determined for the top 50 SFK-responsive phosphorylation sites resulted in an Src-like motif similar to the published motif when only the overexpression experiments were used in the ranking, as compared to when the motif was determined from the drug inhibition experiments (fig. S6). In contrast, the SFK PPI and substrate results were more significant when ranking was based on only the dasatinib drug inhibition experiments (Fig. 3B and table S1). In the analysis where proteins were ranked by drug response scores alone, we also noted a modest enrichment of SH2-containing proteins (table S1). Thus, in addition to affecting SFK activity in opposite directions, SFK overexpression and drug inhibition perturb the signaling network somewhat distinctly and complementarily, with motif-based recognition more strongly affected by overexpression and PPI-based recognition more strongly affected by drug inhibition.

In parallel to the rank-based analysis, we also performed an unsupervised clustering-based analysis of the data (see Supplementary Materials for details), which identified two primary clusters of phosphorylation sites (fig. S7). One cluster was dominated by phosphorylation sites that exhibited increased phosphorylation in response to SFK overexpression and was relatively enriched for Src motifs (table S2). The second cluster was associated with phosphorylation sites that exhibited decreased phosphorylation in the drug experiments and were relatively enriched for SFK PPIs and SH2 domain–containing proteins (table S2).

Our combined rank-based and clustering results suggest that SFK drug inhibition and overexpression perturbation approaches tend to preferentially target protein complex– and Src motif–regulated phosphorylation events, respectively (Fig. 3E).

Activation and overpowering of SFK negative feedback mechanisms by Bcr-Abl signaling

We noticed that several of the top-scoring phosphorylation sites belong to proteins previously characterized as negative regulators of SFKs: Ptpn18,

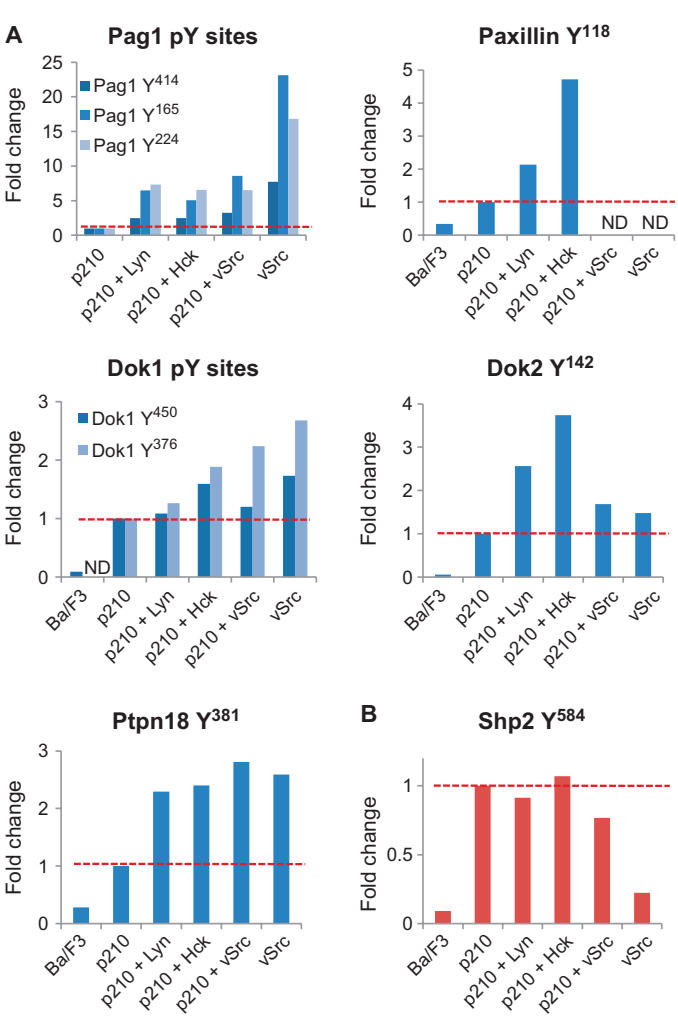

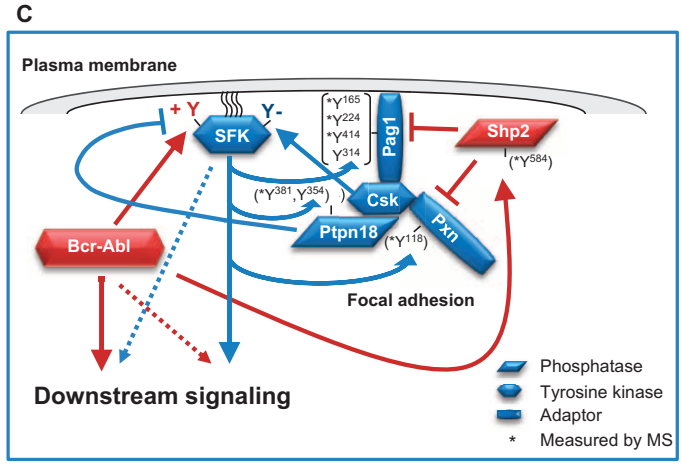

Fig. 4. Bcr-Abl– and SFK-induced tyrosine phosphorylation of proteins involved in negative feedback regulation of SFK activity. (**A**) Tyrosine phosphorylation of proteins that function to inhibit SFK activity. (**B**) Tyrosine phosphorylation of proteins that stimulate SFK activity. In (A) and (B), the phosphorylation of the indicated phosphosites is reported as $\log_2$ fold change with respect to their respective value in the Bcr-Abl (p210 isoform)–expressing Ba/F3 cell line, which was used as a reference and is indicated by the red dotted line. ND, phosphosite values not determined in the indicated sample. The results shown were measured in representative MS runs in which the indicated phosphorylation events were simultaneously detected. All results shown were observed multiple times with the same trends. The abundance of the v-Src protein in Ba/F3 cells (v-Src) is higher than that in the p210 Ba/F3 cells (p210 + vSrc). (**C**) A summary context-specific model of the Bcr-Abl and SFK signaling crosstalk and feedback mechanisms in Bcr-Abl–transformed Ba/F3 cells (red, Bcr-Abl–mediated phosphorylation events; blue, SFK-mediated phosphorylation events). Asterisks indicate phosphorylation events that we detected. Lines ending in arrows indicate a phosphorylation event, and lines ending with a bar indicate a dephosphorylation event. The dotted lines represent signaling crosstalk. Whether the indicated interactions with Csk are individual or co-occurring is unknown.

Pag1, Dok1 and 2, and paxillin (Pxn) (Table 1 and table S3). The overexpression of either Lyn or Hck increased the phosphorylation of three tyrosine residues of the transmembrane phosphoprotein Pag1 (Fig. 4A). This adaptor protein specifically recruits the SFK negative regulator Csk to the plasma membrane (*17*), which leads to the phosphorylation of the C-terminal regulatory tyrosine of SFK, causing the inhibition of its kinase activity. We also found that expression of the constitutively active viral form of Src, v-Src, increased the tyrosine phosphorylation of Pag1 at the same residues, either in the presence or in the absence of Bcr-Abl (Fig. 4A). The overexpression of Lyn and Hck also increased the tyrosine phosphorylation of Pxn at the tyrosine residue Y^{118} (Fig. 4A). Pxn is a multidomain scaffold protein localized at focal adhesions. The phosphorylation of Y^{118} creates binding sites for SH2 domain–containing proteins, including SFKs and Csk (*37*). Lyn, Hck, or v-Src overexpression increased the tyrosine phosphorylation of the adaptor proteins Dok1 and Dok2 at specific residues (Fig. 4A). Dok1 and Dok2 localize to the cytoplasm and bind SFKs and Csk (*38*, *39*). Because the tyrosine phosphorylation of specific residues of Pag1, Pxn, Dok1, and Dok2 has been reported to increase the local concentration of Csk near SFKs, our results overall indicate that Bcr-Abl–transformed cells respond to increased SFK activity by activating Csk-linked negative feedback targeted at the SFK inhibitory site.

Among the tyrosine phosphorylation events at the top of our ranked list, we also observed phosphorylation sites on Ptpn18, a phosphatase that inhibits SFK activity through the dephosphorylation of the positive regulatory tyrosine of the SFK activation domain (*23*). We found that overexpression of Lyn, Hck, or v-Src increased the phosphorylation of Y^{381} of Ptpn18 (Fig. 4A). Furthermore, similar to the phosphorylation of Pag1 and Dok1, v-Src increased the phosphorylation of Ptpn18 Y^{381} independently of Bcr-Abl (Fig. 4A). Thus, these results suggest that Ptpn18 Y^{381}, along with Pag1 Y^{414}, Y^{165}, and Y^{224} and Dok1 Y^{450}

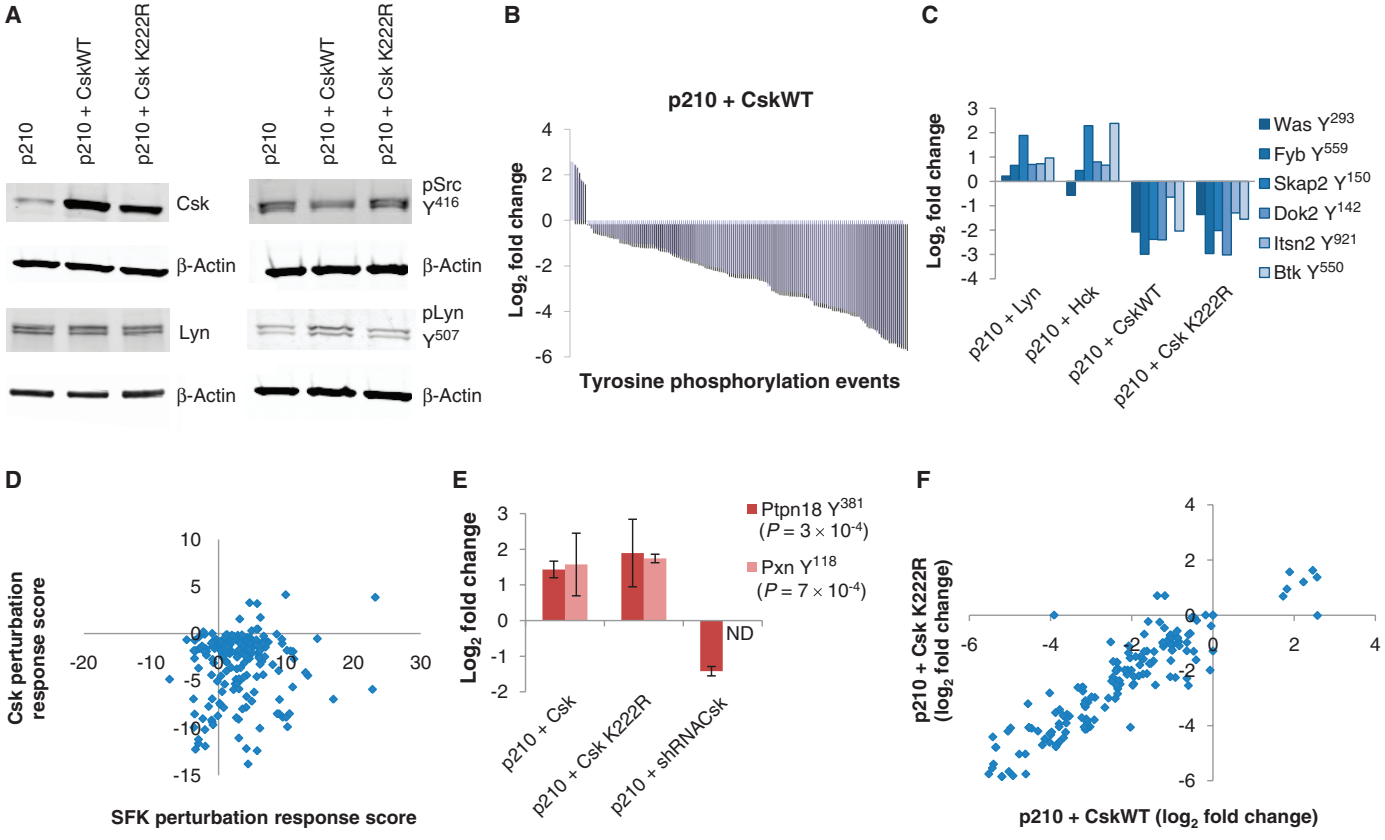

Fig. 5. Csk overexpression mediates a global decrease of tyrosine phosphorylation, independently from its kinase activity. (**A**) Effects of overexpression of wild-type Csk (CskWT) or kinase-deficient Csk K222R on SFK regulatory phosphorylation events. (**B**) Ranked log fold changes of tyrosine phosphorylation events (n = 99) upon Csk overexpression in the p210 Bcr-Abl Ba/F3 cell line. Changes are relative to p210-expressing cells. Data are representative of one of three replicate experiments. (**C**) Log fold changes with respect to the p210 background of SFK-dependent phosphorylation events in different perturbation experiments. These SFK events are a subset of those with high SFK perturbation response scores and identified as SFK substrates and interacting proteins (Table 1). (**D**) The events repressed by Csk overexpression include both SFK perturbation responsive and nonresponsive events, as indicated by the lack of correlation between Csk responsiveness and SFK responsiveness (correlation coefficient R = 0.08). The Csk perturbation response score is defined similarly to the SFK score but with three independently derived replicates of the Csk-overexpressing cell lines (see Materials and Methods). (**E**) Changes in the phosphorylation of Ptpn18 and paxillin (Pax) in Csk overexpression and knockdown experiments as measured by quantitative MS. Results include two independent hairpins targeting Csk (fig. S9). Error bars are SEM. P values are based on comparisons of the observed replicate fold changes to the background fold change distributions from measuring like biological samples (see fig. S12). ND, not determined. (**F**) Scatter plot showing the high correlation (R = 0.9) of phosphorylation event fold changes between cells overexpressing either CskWT or Csk K222R.

and Y^{376}, is an SFK target substrate. Ptpn18 interacts with the SH2 domain of Csk, and the phosphorylation of tyrosines 354 and 381 is critical for this association (*23*). This phosphorylation-regulated interaction with Csk is thought to increase the local concentration of Ptpn18 near active SFK signaling complexes to promote Ptpn18-mediated dephosphorylation of the SFK activation site. Thus, in the Bcr-Abl context, increased SFK activity appears to activate Csk-related feedback mechanisms targeted both at phosphorylation of the SFK inhibitory site and at dephosphorylation of the SFK activation loop.

Because Bcr-Abl activates SFKs (fig. S8) (*40*), we analyzed whether Bcr-Abl expression alone, in the absence of SFK overexpression, also activated these SFK negative feedback mechanisms. In Bcr-Abl–transformed Ba/F3 cells, the phosphorylation of Pxn, Dok1 and 2, and Ptpn18 was induced compared to the parental cells (Fig. 4A). Induction of Pag1 phosphorylation by Bcr-Abl could not be assessed from our data because the signal was below or near background in the parental and Bcr-Abl–expressing Ba/F3 cells, respectively, with induction not detectable until SFKs were overexpressed. These results suggest that SFK negative feedback loops are activated by expression of Bcr-Abl or v-Src alone and that in the presence of Bcr-Abl they are further activated by overexpression of SFKs. We hypothesize that the cell is attempting to down-regulate the oncogene-driven supraphysiological SFK signaling. Nonetheless, this attempt appeared unsuccessful because our global analyses indicated that SFKs remained active, phosphorylating downstream targets, suggesting that additional mechanisms that oppose and overpower the function of the negative feedback loops occur in these cells.

Several possible mechanisms acting through the regulation of tyrosine phosphorylation may counteract the SFK negative feedback loops. The most direct and expected mechanism that opposes the negative feedback loop is the Bcr-Abl–induced phosphorylation of the positive regulatory tyrosine in the activation domain of SFK (fig. S8) (*40*). We also detected a countermeasure to SFK negative feedback loops activated by Bcr-Abl. Bcr-Abl induces the phosphorylation of Y^{584} of the Shp2 (Ptpn11) tyrosine phosphatase (Fig. 4B). Phosphorylation of this residue typically positively influences Shp2 activity (*41*). Shp2 promotes SFK activation by reducing phosphorylation of Pag1, thereby reducing the colocalization of Csk with SFKs (*19*). Additionally, it has been proposed that Shp2 also decreases the phosphorylation of Y^{118} of Pxn, thus reducing the binding of Pxn to Csk (*19*). Phosphorylation of Y^{584} of Shp2 was not increased by Lyn, Hck, or v-Src overexpression in p210 Bcr-Abl Ba/F3 cells, nor by v-Src expression in Ba/F3 cells, further classifying this event as Bcr-Abl–mediated and SFK-independent. Thus, the cooperative role of Shp2 in Bcr-Abl–mediated transformation may be due to derepression of SFK inhibition as well as its potential for enhancement of Bcr-Abl–activated Ras signaling (*19*, *42*, *43*). A summary model of the Bcr-Abl and SFK signaling crosstalk and feedback mechanisms based on our results is shown in Fig. 4C.

Global inhibition of Bcr-Abl signaling by Csk independent from the kinase activity of Csk

Because Csk is a central player in limiting SFK activity, both directly through its ability to phosphorylate the inhibitory residue of SFKs and indirectly through its ability to scaffold proteins such as the phosphatase Ptpn18 that dephosphorylates the activating residue in SFKs, we evaluated Bcr-Abl Ba/F3 cells stably overexpressing this negative SFK regulator or the kinase-deficient mutant form (Csk K222R) (*44*) (Fig. 5A). Two properties make Csk unusual among tyrosine kinases. First, current data indicate that Csk is a highly specific kinase that phosphorylates only the C-terminal tails of SFKs, promoting their inactivation, and this specificity is maintained when Csk is overexpressed (*45*). Second, Csk is not regulated by the phosphorylation of its activation loop and thus is constitutively active (*46*), which indicates that the kinase activity of Csk is mainly regulated by its localization in the cell.

Upon overexpression of Csk in Bcr-Abl Ba/F3 cells, we observed an approximately twofold increase in the phosphorylation of the SFK C-terminal negative regulatory site (Y^{507} in Lyn) and an approximately twofold decrease in SFK activation site phosphorylation (Y^{416} in Src) relative to Bcr-Abl Ba/F3 cells. In contrast, overexpression of the kinase-deficient version Csk K222R had no substantial effect on the amount of phosphorylation of either the SFK activation site (Y^{416}) or the negative regulatory site (Y^{507}) (Fig. 5A). The effect of Csk overexpression on the global tyrosine phosphorylation profiles measured with our quantitative MS assay revealed a twofold or greater decrease in the tyrosine phosphorylation of a large group of phosphorylation sites (72 of 99 total) (Fig. 5B). This effect varied from a mild reduction to a 30-fold decrease relative to Bcr-Abl Ba/F3 cells. Among the targets of these decreased phosphorylation events, we found known SFK substrates (Fig. 5C) and events with high SFK perturbation response scores (events positively correlated with SFK activity) (Fig. 5D), but we also found many Csk-repressed events that had low SFK perturbation response scores (Fig. 5D).

In contrast to the general trend, we observed an increase in the phosphorylation of a small group of five phosphorylation sites upon overexpression of Csk (Fig. 5B). This group included the Y^{381} of Ptpn18 and Y^{118} of Pxn (Fig. 5E). Phosphorylation of Y^{381} of Ptpn18 was decreased in a stable knockdown of Csk in p210 Bcr-Abl Ba/F3 (Fig. 5E and fig. S9). We hypothesize that Csk protects the dephosphorylation of these sites through direct PPIs, which is consistent with previous findings (*23*). Thus, the set of Csk-induced phosphorylation events overlapped with the Ptpn18 and Pxn phosphorylation events that were induced by increased SFK activity (Fig. 4) and were implicated in mediating critical protein-protein physical interactions involved in Csk-mediated regulation of SFK activity (see table S3 for the fold change data of all sites affected by Csk overexpression).

To distinguish between the functions of Csk that are mediated through its catalytic activity from those mediated through its role as an adaptor protein, we compared the phosphorylation changes caused by the kinase-deficient version of Csk (K222R) to those caused by overexpression of wild-type Csk. We found that the global effects on tyrosine phosphorylation mediated by Csk wild-type and Csk K222R were highly correlated (Fig. 5F). Furthermore, the targets of this down-regulation included both candidate phosphorylation events occurring on SFK targets and SFK-independent phosphorylation events as defined by their SFK perturbation response score (Fig. 5, C and D). Thus, we conclude that the overexpression of Csk in p210 Bcr-Abl Ba/F3 cells leads to the inhibition of Bcr-Abl and SFK signaling independently of the kinase activity of Csk and likely depends on its function as an adaptor protein, potentially by recruitment of phosphatases, such as Ptpn18, to the site of SFK activity (Fig. 4C).

Rapid decay of SFK activation and substrate dephosphorylation upon Bcr-Abl inhibition

To further characterize events downstream of Bcr-Abl and SFKs, we inhibited Bcr-Abl with the Abl-targeted inhibitor imatinib (Gleevec) (*7*) and followed the decay kinetics of SFK regulatory phosphorylation events and downstream signaling. We observed an overall rapid decay, within 2 min, of the total phosphotyrosine signal as assayed by pan-specific phosphorylated Tyr immunoblotting (Fig. 6, A and B). Using MS-based phosphoprofiling, we observed multiple clusters of phosphorylation events with a range of decay kinetics, including some nondecaying events (Fig. 6C and table S4). One hypothesis for the range of decay kinetics

observed upon Bcr-Abl inhibition is differential phosphatase regulation of, association with, or access to phosphorylated substrates within the context of the kinase-phosphatase kinetic equilibrium balance. We tested this hypothesis by evaluating whether the rapidly decaying phosphorylation events were more likely to occur on phosphatases and their interacting proteins and substrates (based on HPRD). In this enrichment analysis, we found that the phosphoproteins with the most rapid decay kinetics were enriched for phosphatase-associated proteins (Fig. 6C).

When we assayed the same lysates for the abundance of the SFK regulatory phosphorylation events upon Bcr-Abl inhibition, we found rapid decay of the Src Y^{416} activating phosphorylation that matched the kinetics of overall Tyr phosphorylation, whereas phosphorylation of the C-terminal negative regulatory phosphorylation (as measured by antibodies against Lyn $Y^{507}$and Src Y^{527}) did not decay (Fig. 6B and fig. S10). Bioinformatic enrichment analysis of the MS-measured phosphoproteins, ranked by their decay kinetics, indicated that the rapidly decaying events, which matched the kinetic pattern of pSrcY^{416} dephosphorylation, were enriched for known SFK-interacting proteins and substrates (based on HPRD; Fig. 6C). Together with the observation that the global effects on tyrosine phosphorylation of kinase-deficient Csk were highly similar to those of wild-type Csk in the context of Bcr-Abl signaling (Fig. 5F), these results suggest that SFK-activating phosphorylation is a stronger determinant or indicator of SFK activity in a Bcr-Abl context than is overall SFK inhibitory C-terminal phosphorylation. However,

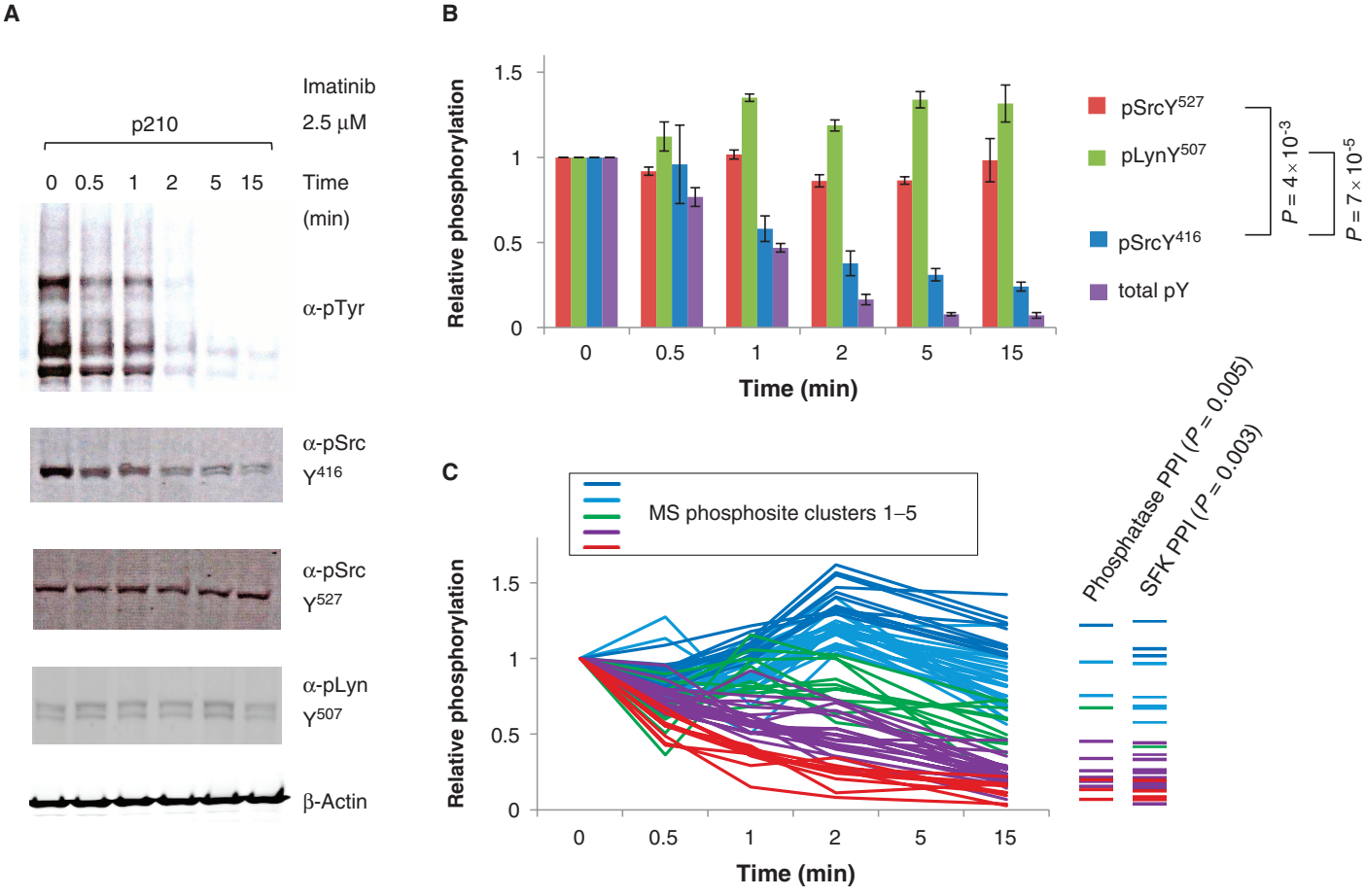

Fig. 6. SFK activation and substrate phosphorylation are associated with rapid decay and dephosphorylation upon Bcr-Abl inhibition. (**A**) Representative immunoblot analysis showing the decay kinetics of total tyrosine phosphorylation detected with antibodies that recognize phosphotyrosine residues (α-pTyr; clone 4G10), antibodies that recognize tyrosine phosphorylation of the SFK activation domain tyrosine (pSrcY^{416}), and antibodies that recognize phosphorylation of the C-terminal negative regulatory tyrosine phosphorylation (pSrcY^{527}, pLynY^{507}) during a time course of inhibition of Bcr-Abl activity with imatinib (Gleevec; 2.5 μM). β-Actin serves as a loading control. (**B**) Quantitative analysis (LI-COR) of replicate immunoblots, including those shown in (A). Each time point is normalized to its corresponding β-actin loading control, and all series are scaled to their initial amounts. Error bars reflect the SEM. *P* values are based on a two-way analysis of variance (ANOVA). (**C**) Amount of cellular phosphorylation events detected by quantitative MS during a 15-min time course of Bcr-Abl inhibition with imatinib. The phosphorylation event decay patterns were grouped by hierarchical clustering. Bioinformatic enrichment analysis was performed on the lists of phosphoproteins ranked by the decay kinetics of their phosphorylation events using the HPRD PPI database. The most rapidly decaying events are enriched both for phosphatases and their interacting proteins and substrates (phosphatase PPI) and for known SFK-interacting proteins and substrates (SFK PPI), as indicated by the ladder plots and associated enrichment *P* values to the right of the graph. The full imatinib kinetic results can be found in table S4.

it remains possible that the kinetic response of C-terminal phosphorylation of the Bcr-Abl–engaged subpopulation of SFKs is masked by other populations of SFKs that are in the inhibitory phosphorylation state.

SFK feedback indicators and sensitivity to Abl inhibition in human CML cell lines

As a preliminary test of the identified SFK regulatory mechanisms as candidates for dysregulation during BCR-ABL–positive leukemia progression and acquisition of ABL inhibitor resistance, we profiled two human CML cell lines with different sensitivities to imatinib. [Note: Nomenclature follows the HUGO convention of all capitals for human proteins and initial capitals for mouse proteins.] We first verified previous reports that the LAMA-84 cell line is more sensitive to imatinib treatment than is the K562 line (*47*, *48*) (Fig. 7A). Upon assessment of the phosphorylation and total amount of SFKs, CSK, and SHP2, we found that, whereas both cell lines had similar amounts of these proteins, their phosphorylation levels differed (Fig. 7B). The abundance of SRC pY^{416} and phosphorylated SHP2 was greater in the LAMA-84 cells. Notably, imatinib exposure substantially reduced the amount of SRC pY^{416} in LAMA-84 cells, whereas K562 cells maintained more constant amounts of SRC pY^{416}. Sustained SRC activity upon BCR-ABL inhibition has been previously reported (*2*). As observed in our kinetic studies (Fig. 6), phosphorylation of the SFK C-terminal negative regulatory site (pY^{527} in SRC or pY^{507} in LYN) did not change upon imatinib treatment. In both LAMA-84 and K562 cells, BCR-ABL inhibition by imatinib resulted in reduction of the amount of phosphorylated SHP2. In K562, this occurred despite sustained SRC active-site phosphorylation, providing further support that SHP2 phosphorylation is a BCR-ABL–mediated, SFK-independent event. These data are consistent with the interpretation based on our phosphorylation profiling–inferred model (Fig. 4C) in which the greater abundance of phosphorylated SHP2 observed in LAMA-84 cells results in suppression of SFK negative feedback mechanisms. Accordingly, inhibition of BCR-ABL results in a decrease in BCR-ABL–mediated phosphorylation of SHP2 and, thus, a release of SHP2-mediated inhibition of the SFK negative feedback mechanisms. Although further studies are required, the apparent greater engagement of this BCR-ABL–mediated pro-signaling mechanism by LAMA-84 cells compared to that in the more imatinib-resistant K562 cells suggests that escape from SHP2-regulated SFK negative feedback mechanisms may result in increased resistance to BCR-ABL inhibition.

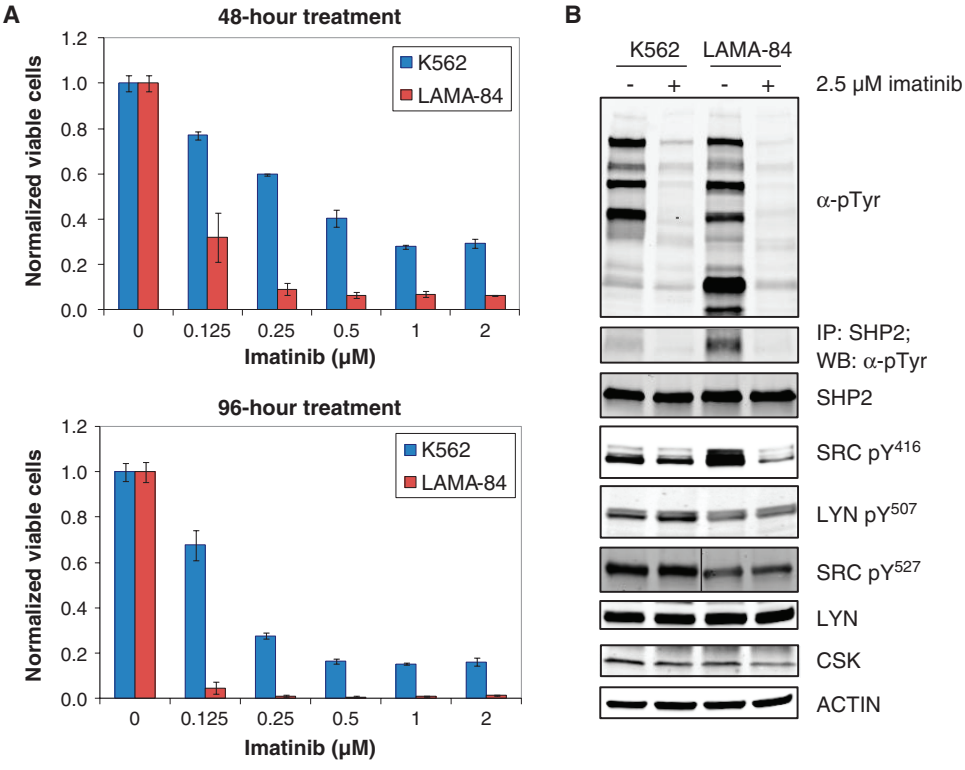

Fig. 7. Differential SFK regulatory activity accompanied by differential imatinib sensitivity in human leukemia cell lines. (**A**) Comparison of imatinib sensitivity of two human leukemia, BCR-ABL–positive cell lines, K562 and LAMA-84 cells. Cell viability is presented as the normalized number of viable cells relative to the untreated control based on trypan blue exclusion. The observed differences between the cell lines are statistically significant based on a two-way ANOVA: $P < 10^{-15}$ for both time points. EC_{50} values were calculated as 0.22 μM for K562 and 0.10 μM for LAMA-84 at 48 hours and 0.14 μM for K562 and 0.01 μM for LAMA-84 at 96 hours. (**B**) Representative analysis of SFK regulatory phosphorylation events in K562 and LAMA-84 cells. Cells were mock-treated (DMSO) or treated with 2.5 μM imatinib for 2 hours, and the cell protein lysates were probed for global tyrosine phosphorylation (4G10 antibody), SHP2 (PTPN11) phosphorylation (immunoprecipitation of SHP2 and immunoblot with 4G10, anti-pTyr antibody), and SFK phosphorylation (SRC pY^{416}, SRC pY^{527}, and LYN pY^{507}; note that these phosphorylation-detecting antibodies cross-react with multiple SFKs due to phosphorylation motif homology). In addition, lysates were probed for total protein abundance of SHP2, LYN, CSK, and ACTIN.

DISCUSSION

Despite the success of the drugs imatinib and dasatinib, subclasses of Bcr-Abl–driven leukemias remain difficult to treat (*3*, *12*), and intrinsic and acquired resistance to pharmacological treatment is often seen in the advanced blast crisis phase of CML and in Bcr-Abl–positive B-ALL (*4*). Several findings have pointed to the relevance of SFKs in distinct subtypes of Ph+ leukemias, as well as their association with resistance to imatinib treatment (*1*, *9*–*11*). Here, we have applied global quantitative phosphorylation approaches (*24*, *49*, *50*) to delineate the structure of Bcr-Abl and SFK signaling networks in a Bcr-Abl–driven cell line model of leukemia and to reveal potential mechanisms of drug resistance.

We found that two different perturbations of the SFK signaling network—stable overexpression of Src family members and drug inhibition of SFK activity—affected overlapping lists of phosphorylation events. However, the lists were enriched for different properties. Our dose-response inhibition experiments with dasatinib tended to perturb phosphorylation sites of proteins enriched for PPIs with SFKs. In contrast,

the overexpression of Lyn or Hck tended to increase the phosphorylation of proteins containing Src motifs. We hypothesize that phosphorylation sites affected by dasatinib treatment (or inhibition of the kinase activity of SFKs in general) commonly belong to proteins that form stable complexes with SFKs and their associated adaptor proteins. On the other hand, the phosphorylation sites that tend to be affected by the overexpression of Lyn and Hck may be phosphorylated through less stable kinase active site–protein phosphorylation site interactions, and therefore, the presence of an Src motif favors their phosphorylation (Fig. 3E). The distinguishable contribution of both motif guidance and protein interaction guidance to kinase specificity has been observed in other targeted and network-wide studies of signal transduction (*51*, *52*).

The unbiased nature of the MS phosphorylation assay allows us to simultaneously measure hundreds of phosphorylation events and their coordinated response to different perturbations with which we reconstructed regulatory circuitry. Examination of our top-ranked SFK-responsive phosphorylation sites and the corresponding literature suggested that several feedback mechanisms regulating SFK activity operate in Bcr-Abl–expressing cells. From the combination of our data and previously reported mechanisms, we defined a model of three SFK negative feedback mechanisms that are activated in Bcr-Abl–expressing hematopoietic cells (Fig. 4G). The core of this model involves the phosphorylation of the phosphatase Ptpn18 and the adaptor proteins Pag1 and Pxn and the interactions of these proteins with the negative regulator Csk. The phosphorylation of Y^{118} of Pxn and Y^{381} of Ptpn18 is critical for stabilizing their interaction with Csk (*19*). Although we did not detect phosphorylation of the Pag1 Y^{314}, which is critical for the recruitment of Csk (*17*, *18*), we did find the coordinated increase in the tyrosine phosphorylation of three other Pag1 residues upon Lyn or Hck overexpression, suggesting that these residues may also play a related role in SFK feedback regulation. Whether Ptpn18, Pxn, Pag1, and Csk act through the formation of one or multiple complexes, or through one or more mechanisms, remains to be determined. Underscoring the potential oncogenic relevance of Csk-centered protein interaction mechanisms for SFK regulation is a report that colon cancer cell invasion is induced by Pag1-mediated membrane delocalization of Csk (*53*).

Because phosphorylation of SFK substrates that are not involved in negative feedback mechanisms also increased upon SFK overexpression, we speculated that a second layer of positive feedback counteracting the negative regulation is operating in Bcr-Abl cells. We propose two mechanisms through which positive regulation occurs. One comes from the constitutive activation of SFKs by Bcr-Abl, which, as previously shown in myeloid cells, may also involve their stable protein-protein association (*40*). A second mechanism may involve the phosphatase Shp2, which increases both SFK activity and Ras-ERK (extracellular signaling–regulated kinase) pathway activation by reducing the recruitment of Csk through the dephosphorylation of Pag1 and Pxn (*19*, *43*) and which has been implicated in Bcr-Abl–mediated transformation (*42*). We observed that the phosphorylation of Shp2 at Y^{584} was increased by Bcr-Abl expression, but SFKs did not appear to mediate this phosphorylation (Fig. 4B). Moreover, this tyrosine residue of Shp2 is a direct substrate of the kinase c-Abl (*54*). Our data suggest that Shp2 becomes activated after its phosphorylation by Bcr-Abl at residue Y^{584} (and possibly other residues) and contributes positively to SFK activation by dephosphorylating Pag1 and Pxn and thus limiting Csk recruitment. Our finding that Bcr-Abl activates Shp2 phosphorylation in an SFK-independent fashion further links the signaling function of Shp2 to its phenotypic consequences in leukemic transformation (*42*).

An interesting role for Csk, the negative regulator of SFK, has emerged from our profiling experiments. Upon Csk overexpression, we observed a consistent decrease of a large number of phosphorylation events as well as an increase in the tyrosine phosphorylation of a small group of phosphorylation sites. Among the down-regulated sites, we found both SFK-dependent and SFK-independent phosphorylation events (Fig. 5D). Unexpectedly, we found that this global inhibitory effect on tyrosine phosphorylation was not dependent on the kinase activity of Csk because the kinase-deficient version of Csk (the K222R mutant form) generated a similar profile (Fig. 5F), suggesting that Csk functions in this context primarily as an adaptor protein. The SH2 and SH3 domains of Csk, in addition to the kinase domain, are important for regulating its inhibitory function (*55*). The SH3 domain permits Csk association with tyrosine phosphatases PEP and PTP-PEST (*56*), whereas the SH2 domain interacts with the tyrosine phosphatase Ptpn18 (*23*). Because we observed that SFK perturbations affected the tyrosine phosphorylation of Ptpn18, we hypothesize that Ptpn18 may mediate the system-wide phosphotyrosine down-regulation observed upon Csk overexpression (Fig. 5B). In fact, Ptpn18 Y^{381} is among the few phosphorylation events that increased upon Csk overexpression of both the wild-type protein and the kinase-deficient mutant, which is consistent with previous observations that suggest binding to Csk protects Ptpn18 from dephosphorylation (*23*). Increased Csk abundance may increase the local concentration of Ptpn18, and possibly other phosphatases, by mediating their recruitment to foci of SFK activity. Our results suggest that, at least in the context of a Bcr-Abl–driven leukemia system, Csk exerts an inhibitory function on tyrosine phosphorylation through its adaptor properties as well as through its kinase activity. Kinase-independent mechanisms of repression of SFK signaling by the Csk family member, Chk (*57*), and adaptor-like functions of other kinases, such as the kinase Zap70 (*58*), have also been identified.

We also observed that in a Bcr-Abl context the phosphorylation of the C-terminal tyrosine residue of SFK was not a strong indicator of SFK activity. In vitro, autophosphorylation of Src family members Src and Yes can block their inactivation by Csk phosphorylation (*59*). In vivo, the phosphorylation of the activation domain tyrosine antagonizes inhibition by increasing the accessibility of the SH3 domain to non-self protein interactions (*60*), leading to a model in which an SFK, once activated, may be less prone to C-terminal inhibitory site regulation so that an initial input signal produces a positive feedback regulation of SFK activity (*60*). In Ph+ leukemias, Bcr-Abl provides a high and constant source of activation for SFK. Thus, the constitutive activity of Bcr-Abl may provide a context in which the phosphorylation of the C-terminal negative regulatory tyrosine is a less efficient mechanism for regulating SFK activity than other mechanisms that directly modulate the phosphorylation status of the SFK activation domain tyrosine, such as through Ptpn18.

Despite the clear induction of several SFK negative feedback mechanisms by Bcr-Abl, Src signaling undergoes a net activation upon the introduction of the *Bcr-Abl* oncogene (fig. S8) (*40*). Although Bcr-Abl activation of SFK signaling outweighs SFK negative feedback mechanisms, SFK signaling can still be reduced by enhancing the negative feedback pathways, as exemplified by the reduced SFK substrate phosphorylation upon increased expression of Csk (Fig. 5C). These results suggest that increased SFK signaling in subsets of Bcr-Abl–driven leukemias may, in part, be due to deficiencies in SFK negative feedback acquired during tumor progression and acquisition of drug resistance (*10*, *18*, *53*, *61*). Examination of two human CML cell lines with differential imatinib sensitivity provided preliminary support for this candidate resistance mechanism (Fig. 7).

The network-wide perturbation and phosphorylation profiling approach allowed us to reconstruct portions of the Bcr-Abl and SFK

signaling network that are active in the context of a model of Bcr-Abl–driven leukemia. The application of this approach to other leukemia contexts should help delineate rewiring of the network during disease progression and acquisition of drug resistance and delineate network differences between different hematopoietic lineages with distinct clinical leukemia characteristics. The signaling events described here offer candidate targets for molecular diagnostics and therapies related to SFK involvement in Bcr-Abl–driven leukemias.

MATERIALS AND METHODS

Plasmids, antibodies, and kinase inhibitors

The pMSCVneo-Lyn and pMSCVneo-Hck plasmids were generated by subcloning the full-length corresponding human complementary DNA (cDNA) (IRAT-IRAU collections from Open Biosystems, Thermo Scientific), respectively, into the Eco RI and Eco RI–Xho I sites of the pMSCVneo retroviral vector (Clontech). A 2.1-kb fragment, obtained by partial Eco RI digestion of the pCR4-TOPO plasmid (IRAT collection, Open Biosystems) and containing the full-length human cDNA of Csk, was inserted into the Eco RI site of the pMSCVneo vector to generate the pMSCVneo-Csk plasmid. pMSCVneo-Csk was used as template for site-directed mutagenesis performed with the QuikChange mutagenesis kit (Stratagene) to generate the pMSCVneo-CSKK222R mutant plasmid. The pMSCVpuro-p210Bcr-Abl plasmid and the pMSCVpuro-p210T315A and pMSCVpuro-p210T315I mutant constructs have been reported elsewhere (*28*). pMSCVpuro-vsrc was created by polymerase chain reaction (PCR) amplification of the *env* and *v-src* coding sequences from pMvsrc (a gift from H. Herschman) (*62*) and subcloning this insert into the Bgl II and Xho I sites of pMSCVpuro (Clontech). The pMSCVneo-p210Bcr-Abl plasmid, used to generate the p210 Ba/F3 neomycin-resistant cell line recipient for knockdown experiments, was made by subcloning the 6.9-kb Eco RI fragment from the pMSCVpuro-p210Bcr-Abl plasmid into the same site of pMSCVneo vector. The LMP-CskShRNA plasmid used for knockdown experiments was generated by subcloning two separate microRNA-adapted hairpins directed toward Csk, shRNAmir (Open Biosystems), from the PSM2 vector (Open Biosystems) into the Eco RI/Xho I sites of the LMP retroviral vector (puromycin resistance; Open Biosystems). The hairpin sequences are TGCTGTTGACAGTGAGCG-**CGGGCATCATCCCAGCCAACTA**TAGTGAAGCCACAGATGTA-TAGTTGGCTGGGATGATGCCCTTGCCTACTGCCTCGGA (ShRNACsk1) and TGCTGTTGACAGTGAGCG**ACCTTGTGA-GATGGAATCAATA**TAGTGAAGCCACAGATGTATATTGATTC-CATCTCACAAGGCTGCCTACTGCCTCGGA (ShRNACsk2). Bold letters indicate the postprocessing 22-nucleotide microRNA. In each case, all constructs were transiently transfected by the calcium phosphate method into 293T cells to assess by immunoblot either the correct protein expression or the knockdown efficiency. Antibodies used for immunoblot analysis include antibodies that recognize Lyn or Csk (Santa Cruz Biotechnology); pSrcY^{416}, pLynY^{507}, or pSrcY^{527} (Cell Signaling); phosphotyrosine (clone 4G10, Upstate-Millipore); and actin (Sigma-Aldrich). Immunoblots were quantitatively analyzed by Odyssey Infrared Imaging System (LI-COR). The kinase inhibitors used in this work, dasatinib (BMS-354825) and Gleevec (STI571) (both from ChemieTek), were both prepared as 20 mM stock solutions in dimethyl sulfoxide (DMSO). Stock solutions were diluted in cell culture media and added directly to cells. The final concentration of DMSO was 0.0025% in the dose-response experiments and 0.00125% in the time course kinetic experiments across all samples.

Cell lines and culture

Pro-B, lymphoid, Ba/F3 cells transformed with the wild-type, T315A, and T315I isoforms of Bcr-Abl p210 have been described previously (*24*). These cells display similar amounts of Bcr-Abl abundance and signaling as Ph+ patient leukemia primary samples. Stable overexpression of Lyn, Hck, Csk, or Csk K222R, or stable knockdown of Csk in the p210 Ba/F3 cell line, was obtained by retroviral infection of the corresponding virus-containing supernatant as previously described (*28*). High infection efficiency was achieved by infecting 0.5×10^6 p210 Ba/F3 cells with 3 ml of undiluted viral supernatant, collected at 48 hours, through spinduction (1800 rpm, 90 min at 34°C) in the presence of polybrene (4 mg/ml). Lower infection efficiency, resulting in lower overexpression of Lyn and Hck, was obtained by omitting the spinduction step and infecting 2×10^6 p210 Ba/F3 cells. Infected cells were selected for at least 2 weeks in RPMI 1640 medium (Cellgro, Mediatech) with 10% fetal bovine serum (FBS) (Omega Scientific) and penicillin/streptomycin in the presence of either G418 (1 mg/ml; Sigma) or puromycin (1 mg/ml; Sigma). Cells were cultured in the presence of antibiotic also during expansion before MS analysis. Cell lysates for immunoblot and MS analysis were lysed by sonication in urea buffer [8 M urea, 50 mM tris-HCl (pH 7.5), and 1 mM vanadate]. The K562 and LAMA-84 CML cell lines were obtained from DMSZ.

Drug inhibition kinetic and dose-escalation experiments

To measure the short-term (de)phosphorylation kinetics after imatinib treatment, we adapted a protocol with a rapid ethanol-fixation step (*63*). For this, p210 Bcr-Abl Ba/F3 cells were grown in RPMI medium with 10% FBS. The medium was replaced with fresh RPMI supplemented with 0.5% FBS to prevent serum protein precipitation in the ethanol-fixation step. After 1 hour of equilibration time, the time course was initiated by the addition of 2.5 μM imatinib or the respective volume of the solvent (DMSO). At the indicated time points, the incubation was terminated rapidly by addition of 80% (v/v) ethanol at −20°C. The cells were collected by centrifugation, washed with phosphate-buffered saline (PBS), and lysed by sonication in urea buffer. For cellular drug sensitivity experiments, 2×10^5 cells/ml were plated with the indicated concentrations of imatinib, and cell viability was assessed after 48 and 96 hours by trypan blue exclusion. The EC_{50} for normalized viable cells was determined with the drc analysis package (*64*). In all dose escalation panels, each sample was treated with a single dose for the indicated amount of time.

Phosphopeptide immunoprecipitation, quantitative analysis by MS/MS, and identification by fragmentation spectra sequencing and chromatography alignment

Bcr-Abl p210 Ba/F3 cells expressing various control, SFK, and Csk plasmids were grown, processed, and analyzed by MS two to four times independently. Phosphotyrosine peptide immunoprecipitation was performed with pan-specific anti-phosphotyrosine antibodies (clone 4G10, Millipore) using 2×10^8 cells (30 mg of total protein) as previously described (*24*, *26*).

Phosphorylated peptides were analyzed by LC-MS/MS with an Eksigent autosampler coupled with a Nano2DLC pump (Eksigent) and LTQ-Orbitrap (Thermo Fisher Scientific). The samples were loaded onto an analytical column (10 cm, 75 μm inside diameter) packed with 5 μm Integrafit Proteopep2 300 Å C18 (New Objective). Peptides were eluted into the mass spectrometer with a high-performance liquid chromatography (HPLC) gradient of 5 to 40% buffer B in 45 min followed by a quick gradient of 40 to 90% buffer B in 10 min, where buffer A contained 0.1% formic acid in water and buffer B contained 0.1% formic acid in acetonitrile. All HPLC

solvents were Ultima Gold quality (Fisher Scientific). Mass spectra were collected in positive ion mode with the Orbitrap for parent mass determination and with the LTQ for data-dependent MS/MS acquisition of the top five most abundant peptides. Each sample was analyzed twice (replicate runs), and in each run one-half of the sample was injected. MS/MS fragmentation spectra were searched with SEQUEST (Version v.27, rev. 12, Thermo Fisher Scientific) against a database containing the combined human-mouse International Protein Index (IPI) protein database (downloaded December 2006 from ftp.ebi.ac.uk). Search parameters included carbamidomethyl cysteine (*C) as a static modification. Dynamic modifications included phosphorylated tyrosine, serine, or threonine (pY, pS, pT, respectively) and oxidized methionine (*M). Results derived from database searching were filtered using the following criteria: Xcorr >1.0(+1), 1.5(+2), 2(+3); peptide probability score <0.001; dCn >0.1; and mass accuracy <5 ppm (parts per million) with Bioworks version 3.2 (Thermo Electron Corp.). Samples TAdasa(1) and TAdasa(2) were processed with a QSTAR XL (Applied Biosystems) mass spectrometer and Mascot database search engine (Matrix Science)–based MSDB database searches as previously described (*24*, *26*). We estimated the false-positive rate of sequence assignments at 0.5% on the basis of a composite target-reversed decoy database search strategy (*65*). A score was used to more accurately localize the phosphate on the peptide (*66*).

As is common in data-dependent MS2 fragmentation sequencing, some peptides identified by sequencing in one sample may not be sequenced or identified in another sample even if the peak is present. Peptide peaks sequenced in some samples but not in others were located in the remaining samples by aligning the chromatogram elution profiles by means of a dynamic time warping algorithm (*67*). An extended explanation of the strategy used in this work, and example performance results, can be found in the supporting information of Zimman *et al*. (*26*).

Relative amounts of the same phosphopeptide across samples run together were determined with custom software from our laboratory to integrate the area under the unfragmented (MS1) monoisotopic peptide peak (*24*, *26*). All peaks corresponding to phosphosites discussed in the text were inspected manually, and any errors in the automated quantitation were corrected. Thirteen percent of more than 20,000 phosphopeptide peaks were randomly chosen and inspected manually, and less than 3% of these were found to have greater than 20% errors in their quantitative values. Note that the changes in the abundance of phosphopeptides observed with the pan-specific anti-phosphotyrosine–based purification and MS could be influenced by posttranslational modifications occurring on residues neighboring the site of phosphorylation that are still within the anti-phosphotyrosine antibody epitope footprint. This possibility should be kept in mind when interpreting or validating such results.

Figures S11 and S12 show a schematic of the MS analysis pipeline and examples of peak alignments and quantitation results (fig. S11) and global changes in the amount of phosphorylation upon SFK perturbation compared to differences between biological replicates (fig. S12). Figure S13 shows unsupervised clustering of phosphorylation profiles from independently derived biological replicates. The Cluster and TreeView programs were used to cluster and visualize the phosphorylation profiling data as heat maps (*68*).

Stable isotope labeling by amino acids in cell culture for phosphopeptide analysis

For comparison to our label-free phosphopeptide quantification method, we adapted a stable isotope labeling by amino acids in cell culture (SILAC) phosphoprofiling experiment combining general SILAC guidelines (*69*, *70*) and our own phosphopeptide enrichment protocol. Light SILAC RPMI medium was prepared by adding 10% (v/v) dialyzed FBS (Omega Scientific), L-methionine (15 mg/liter; Sigma), L-arginine (200 mg/liter; Sigma), and L-lysine (40 mg/liter; Sigma) to RPMI 1640 medium deficient in methionine, arginine, and lysine (Caisson Laboratories). For heavy SILAC RPMI medium, light L-arginine was replaced with an equimolar amount of heavy L-arginine ($^{13}C_6$, $^{15}N_4$; +10.00827 daltons; Sigma), and light L-lysine with an equimolar amount of heavy L-lysine ($^{13}C_6$, $^{15}N_2$; +8.01420 daltons; Cambridge Isotope Laboratories).

Incorporation of SILAC amino acids and conversion of arginine to proline was tested with culture media with four different concentrations of heavy L-arginine that were equimolar to light L-arginine (100, 150, 200, and 275 mg/liter) and the standard concentration of heavy L-lysine. Ba/F3 cells expressing both Bcr-Abl and Csk (p210 + Csk cells) that were adapted to light SILAC RPMI medium were (i) split 1:10 to heavy SILAC RPMI medium, incubated for 2 days; (ii) split 1:50, incubated for 3 days; and (iii) after 3 more days, split 1:2 each day (10+ doublings). Cells were lysed with mRIPA buffer [1% NP-40, 0.25% sodium deoxycholate, 0.15 M NaCl, 1 mM EDTA, 50 mM tris (pH 7.4), and proteinase and phosphatase inhibitors]. Protein (50 μg) was separated by SDS–polyacrylamide gel electrophoresis (SDS-PAGE), the gel was Coomassie-stained, and clearly stained bands were excised and subjected to an in-gel digestion protocol (*71*). Mass spectrometric analysis and MS2 fragmentation–based peptide identification were done as described above. For evaluation, the MS1 peak integration areas of heavy- and light-isotope peptide ions were compared manually, and the heavy amino acid incorporation rate was 97.2 ± 0.5%. Only a slight difference in arginine-to-proline conversion was observed for the four different arginine concentrations, and thus, the standard concentration of L-arginine (200 mg/liter; refers to the molecular weight of light amino acid) was used for the subsequent phosphoprofiling experiments. At this L-arginine concentration, the arginine-to-proline conversion rate was 5.4 ± 0.3%.

Ba/F3 cells expressing both Bcr-Abl and either an empty pMSCVpuro vector (p210 vector control cells) or Csk (p210 + Csk cells) that had been adapted to light SILAC RPMI medium were expanded in two biological replicates following the cell culture procedure described above for the incorporation determination experiment: p210 cells were expanded in light SILAC RPMI medium and p210 + Csk cells in heavy SILAC RPMI medium. Cells were harvested as in our previously described label-free protocol (*24*, *26*). For each replicate, 40 mg of p210 (light isotope–labeled) and 40 mg of p210 + Csk (heavy isotope–labeled) were combined before the reduction, alkylation, trypsinization, and subsequent phosphopeptide purification steps.

Phosphorylated peptides from each of two independent tissue culture and expansion replicates were analyzed in two technical replicate runs each by LC-MS/MS. Search parameters were as described above with the addition of the dynamic modifications for heavy-isotope arginine (+10.00827 daltons) and lysine (+8.01420 daltons). For quantification of the heavy- and light-isotope peptide ions, the same quantification pipeline as for the label-free approach was used—with the adjustment that for each peptide ion both the light and the corresponding heavy elution peak were integrated. A comparison of label-free and SILAC isotope–based quantitative MS results showed strong agreement (R = 0.95) (fig. S14, A to C).

Data analysis

The number of unique phosphorylation sites identified in our experiments was determined by collapsing multiple phosphopeptide ions representing the same phosphorylation site. Multiple detections of the same phosphosite include phosphopeptides of different ion charge state, modification (for example, oxidized methionine), and miscleavage by trypsin. Multiple

detections were compared to ensure no disagreement in trend, and the MS ion with the highest intensity across the samples in an experimental batch was kept as representative for subsequent data analysis. The residue numbers listed for phosphosites correspond to the indicated IPI accession number. Consensus phosphorylation motifs were calculated with WebLogo (*72*).

Perturbation response score–based ranking

Phosphorylation sites were ranked on the basis of their SFK perturbation response score determined by summing the log of the fold change in the SFK activation experiments (SFK overexpression) and subtracting the sum of the log fold change in the low-dose samples (5 and 25 nM) of the SFK drug inhibition experiments. Thus, phosphorylation events with a high score tend to be induced when SFK activity is increased and repressed when activity is inhibited. Phosphorylation events with a low score are anticorrelated with SFK activity, and those with a score relatively close to zero are unresponsive to SFK perturbation. When indicated, only the SFK overexpression or only the SFK drug inhibition experiments were used to determine a subscore. The drug sensitivity scores of Fig. 1C are such an example. The Csk perturbation response score was similarly defined using the Csk overexpression experiments. Phosphosites were ranked by their individual perturbation response scores, and for protein-oriented analysis, proteins were ranked by the average perturbation response score for all phosphosites detected on the protein. Estimated *P* values for the observed fold changes used in the calculation of perturbation scores are based on the like sample distributions in fig. S12, using Fisher's method to combine individual *P* values (*73*) and Benjamini and Hochberg multiple hypothesis false discovery rate (FDR) correction (*74*).

Enrichment analysis for SFK substrates, interacting proteins, and motifs

Perturbation response score–based ranked lists of phosphosites and phosphoproteins were analyzed to test whether the more SFK perturbation responsive events were enriched for SFK-related properties. Phosphosite lists were analyzed for enrichment of phosphosites that contain the consensus "Src Kinase" phosphorylation motif as defined by the Scansite resource using low stringency (*34*). Protein lists were analyzed for enrichment of SFK protein-protein functionally interacting (PPI) proteins and SFK substrates [based on the HPRD database (*33*)] and SH2 domain–containing proteins [based on the InterPro database (*35*)]. In the HPRD database, SFK substrates are a subset of the SFK PPI set. The statistical significance of enrichment was determined by "hypergeometric distribution–based permutation analysis." Ranked lists annotated with the presence or absence of the SFK property of interest were scanned using all possible rank thresholds for the point of maximal enrichment as defined by the minimal hypergeometric distribution–based *P* value. Permutation analysis was then performed by randomly reassigning the perturbation response scores used for ranking and repeating the full analysis, including the calculations of average protein response score when analyzing protein-oriented lists and the scanning of all thresholds. The fraction of permutation cases resulting in a minimum hypergeometric *P* value less than or equal to the observed minimum value was then defined as the permutation-based frequency of random occurrence, that is, the permutation-based *P* value. This procedure is analogous to the permutation approach used in Gene Set Enrichment Analysis (*75*). Comparison permutation *P* values for the likelihood of the observed difference in *P* value between the drug inhibition and overexpression cases were calculated as the fraction of permutation cases where the absolute value of the difference in drug and overexpression log *P* values was lower than in the observed case. Because proteins with negative average SFK perturbation response scores were also found to be slightly enriched for SH2 domains, for this enrichment analysis proteins were ranked by the absolute value of their response scores. Phosphorylation events on exogenously added proteins (Lyn, Hck) were excluded from the enrichment analysis.

SUPPLEMENTARY MATERIALS

www.sciencesignaling.org/cgi/content/full/4/166/ra18/DC1

Analysis: Unsupervised Hierarchical Clustering

Fig. S1. Phosphoproteomics approach to delineate the bifurcation and coupling of the Bcr-Abl and Src family kinase (SFK) signaling network.

Fig. S2. Global quantitative phosphoprofiling of dasatinib dose-escalation experiments reveals phosphorylation events with distinct inhibitor sensitivities and response patterns.

Fig. S3. Comparison of dasatinib dose-response results using wild-type Bcr-Abl (p210) versus dasatinib-resistant T315A Bcr-Abl.

Fig. S4. SFK-related properties are more enriched than Abl-related properties when phosphorylation events are ranked by their SFK perturbation response score.

Fig. S5. The network of PPIs between the 40 proteins associated with the top-ranked SFK perturbation–correlated phosphosites and the 40 proteins with the smallest change in response to SFK perturbation.

Fig. S6. The consensus sequence motifs of the top 50 correlated phosphosites based on SFK overexpression, drug inhibition (dasatinib), and combined rankings.

Fig. S7. Unsupervised hierarchical clustering analysis of the Bcr-Abl and SFK network perturbation data.

Fig. S8. The constitutive kinase activity of Bcr-Abl induces increased phosphorylation of the SFK activation domain tyrosine in Ba/F3 pro-B lymphoid cells.

Fig. S9. Stable Csk knockdown in Ba/F3 Bcr-Abl (p210) cells.

Fig. S10. Phosphorylation of the activation domain and C-terminal tyrosines of SFKs in response to a time course treatment with imatinib.

Fig. S11. MS alignment and quantitation analysis pipeline and representative examples.

Fig. S12. Global changes in phosphorylation amounts upon SFK perturbation compared to differences between biological replicates.

Fig. S13. Global phosphorylation changes detected in independently derived biological replicates are sufficient to correctly cluster like samples in an unsupervised fashion.

Fig. S14. Comparison of label-free and SILAC-based MS quantitation and representative examples.

Table S1. Enrichment of SFK-related properties at the top of our SFK perturbation response score–ranked lists.

Table S2. SFK-related properties of the two clusters generated by the unsupervised hierarchical clustering analysis.

Table S3. Quantitative fold change values for 493 phosphorylation sites upon SFK perturbation by genetics and inhibitors (Excel file).

Table S4. Kinetic fold change values for 74 phosphorylation sites upon imatinib inhibition of Bcr-Abl (Excel file).

References

REFERENCES AND NOTES

1. Y. Hu, Y. Liu, S. Pelletier, E. Buchdunger, M. Warmuth, D. Fabbro, M. Hallek, R. A. Van Etten, S. Li, Requirement of Src kinases Lyn, Hck and Fgr for *BCR-ABL1*-induced B-lymphoblastic leukemia but not chronic myeloid leukemia. *Nat. Genet.* **36**, 453–461 (2004).
2. Y. Hu, S. Swerdlow, T. M. Duffy, R. Weinmann, F. Y. Lee, S. Li, Targeting multiple kinase pathways in leukemic progenitors and stem cells is essential for improved treatment of Ph^+ leukemia in mice. *Proc. Natl. Acad. Sci. U.S.A.* **103**, 16870–16875 (2006).
3. M. Talpaz, N. P. Shah, H. Kantarjian, N. Donato, J. Nicoll, R. Paquette, J. Cortes, S. O'Brien, C. Nicaise, E. Bleickardt, M. A. Blackwood-Chirchir, V. Iyer, T. T. Chen, F. Huang, A. P. Decillis, C. L. Sawyers, Dasatinib in imatinib-resistant Philadelphia chromosome–positive leukemias. *N. Engl. J. Med.* **354**, 2531–2541 (2006).
4. F. Guilhot, J. Apperley, D. W. Kim, E. O. Bullorsky, M. Baccarani, G. J. Roboz, S. Amadori, C. A. de Souza, J. H. Lipton, A. Hochhaus, D. Heim, R. A. Larson, S. Branford, M. C. Muller, P. Agarwal, A. Gollerkeri, M. Talpaz, Dasatinib induces significant hematologic and cytogenetic responses in patients with imatinib-resistant or -intolerant chronic myeloid leukemia in accelerated phase. *Blood* **109**, 4143–4150 (2007).
5. T. A. Carter, L. M. Wodicka, N. P. Shah, A. M. Velasco, M. A. Fabian, D. K. Treiber, Z. V. Milanov, C. E. Atteridge, W. H. Biggs III, P. T. Edeen, M. Floyd, J. M. Ford, R. M. Grotzfeld, S. Herrgard, D. E. Insko, S. A. Mehta, H. K. Patel, W. Pao, C. L. Sawyers, H. Varmus, P. P. Zarrinkar, D. J. Lockhart, Inhibition of drug-resistant mutants of ABL, KIT, and EGF receptor kinases. *Proc. Natl. Acad. Sci. U.S.A.* **102**, 11011–11016 (2005).

6. M. W. Karaman, S. Herrgard, D. K. Treiber, P. Gallant, C. E. Atteridge, B. T. Campbell, K. W. Chan, P. Ciceri, M. I. Davis, P. T. Edeen, R. Faraoni, M. Floyd, J. P. Hunt, D. J. Lockhart, Z. V. Milanov, M. J. Morrison, G. Pallares, H. K. Patel, S. Pritchard, L. M. Wodicka, P. P. Zarrinkar, A quantitative analysis of kinase inhibitor selectivity. *Nat. Biotechnol.* **26**, 127–132 (2008).
7. B. J. Druker, S. Tamura, E. Buchdunger, S. Ohno, G. M. Segal, S. Fanning, J. Zimmermann, N. B. Lydon, Effects of a selective inhibitor of the Abl tyrosine kinase on the growth of Bcr-Abl positive cells. *Nat. Med.* **2**, 561–566 (1996).
8. M. A. Fabian, W. H. Biggs III, D. K. Treiber, C. E. Atteridge, M. D. Azimioara, M. G. Benedetti, T. A. Carter, P. Ciceri, P. T. Edeen, M. Floyd, J. M. Ford, M. Galvin, J. L. Gerlach, R. M. Grotzfeld, S. Herrgard, D. E. Insko, M. A. Insko, A. G. Lai, J. M. Lelias, S. A. Mehta, Z. V. Milanov, A. M. Velasco, L. M. Wodicka, H. K. Patel, P. P. Zarrinkar, D. J. Lockhart, A small molecule–kinase interaction map for clinical kinase inhibitors. *Nat. Biotechnol.* **23**, 329–336 (2005).
9. Y. Dai, M. Rahmani, S. J. Corey, P. Dent, S. Grant, A Bcr/Abl-independent, Lyn-dependent form of imatinib mesylate (STI-571) resistance is associated with altered expression of Bcl-2. *J. Biol. Chem.* **279**, 34227–34239 (2004).
10. N. J. Donato, J. Y. Wu, J. Stapley, G. Gallick, H. Lin, R. Arlinghaus, M. Talpaz, BCR-ABL independence and LYN kinase overexpression in chronic myelogenous leukemia cells selected for resistance to STI571. *Blood* **101**, 690–698 (2003).
11. T. Ito, H. Tanaka, A. Kimura, Establishment and characterization of a novel imatinib-sensitive chronic myeloid leukemia cell line MYL, and an imatinib-resistant subline MYL-R showing overexpression of Lyn. *Eur. J. Haematol.* **78**, 417–431 (2007).
12. P. Ramirez, J. F. DiPersio, Therapy options in imatinib failures. *Oncologist* **13**, 424–434 (2008).
13. J. Wu, F. Meng, L. Y. Kong, Z. Peng, Y. Ying, W. G. Bornmann, B. G. Darnay, B. Lamothe, H. Sun, M. Talpaz, N. J. Donato, Association between imatinib-resistant *BCR-ABL* mutation-negative leukemia and persistent activation of LYN kinase. *J. Natl. Cancer Inst.* **100**, 926–939 (2008).
14. A. Ptasznik, Y. Nakata, A. Kalota, S. G. Emerson, A. M. Gewirtz, Short interfering RNA (siRNA) targeting the Lyn kinase induces apoptosis in primary, and drug-resistant, BCR-ABL1(+) leukemia cells. *Nat. Med.* **10**, 1187–1189 (2004).
15. E. Ingley, Src family kinases: Regulation of their activities, levels and identification of new pathways. *Biochim. Biophys. Acta* **1784**, 56–65 (2008).
16. S. M. Thomas, J. S. Brugge, Cellular functions regulated by Src family kinases. *Annu. Rev. Cell Dev. Biol.* **13**, 513–609 (1997).
17. M. Kawabuchi, Y. Satomi, T. Takao, Y. Shimonishi, S. Nada, K. Nagai, A. Tarakhovsky, M. Okada, Transmembrane phosphoprotein Cbp regulates the activities of Src-family tyrosine kinases. *Nature* **404**, 999–1003 (2000).
18. C. Oneyama, T. Hikita, K. Enya, M. W. Dobenecker, K. Saito, S. Nada, A. Tarakhovsky, M. Okada, The lipid raft-anchored adaptor protein Cbp controls the oncogenic potential of c-Src. *Mol. Cell* **30**, 426–436 (2008).
19. S. Q. Zhang, W. Yang, M. I. Kontaridis, T. G. Bivona, G. Wen, T. Araki, J. Luo, J. A. Thompson, B. L. Schraven, M. R. Philips, B. G. Neel, Shp2 regulates SRC family kinase activity and Ras/Erk activation by controlling Csk recruitment. *Mol. Cell* **13**, 341–355 (2004).
20. T. Brdicka, D. Pavlistová, A. Leo, E. Bruyns, V. Korinek, P. Angelisová, J. Scherer, A. Shevchenko, I. Hilgert, J. Cerný, K. Drbal, Y. Kuramitsu, B. Kornacker, V. Horejsí, B. Schraven, Phosphoprotein associated with glycosphingolipid-enriched microdomains (PAG), a novel ubiquitously expressed transmembrane adaptor protein, binds the protein tyrosine kinase csk and is involved in regulation of T cell activation. *J. Exp. Med.* **191**, 1591–1604 (2000).
21. T. Shima, S. Nada, M. Okada, Transmembrane phosphoprotein Cbp senses cell adhesion signaling mediated by Src family kinase in lipid rafts. *Proc. Natl. Acad. Sci. U.S.A.* **100**, 14897–14902 (2003).
22. L. A. Cary, J. A. Cooper, Molecular switches in lipid rafts. *Nature* **404**, 945, 947 (2000).
23. B. Wang, S. Lemay, S. Tsai, A. Veillette, SH2 domain-mediated interaction of inhibitory protein tyrosine kinase Csk with protein tyrosine phosphatase-HSCF. *Mol. Cell. Biol.* **21**, 1077–1088 (2001).
24. B. J. Skaggs, M. E. Gorre, A. Ryvkin, M. R. Burgess, Y. Xie, Y. Han, E. Komisopoulou, L. M. Brown, J. A. Loo, E. M. Landaw, C. L. Sawyers, T. G. Graeber, Phosphorylation of the ATP-binding loop directs oncogenicity of drug-resistant BCR-ABL mutants. *Proc. Natl. Acad. Sci. U.S.A.* **103**, 19466–19471 (2006).
25. J. Rush, A. Moritz, K. A. Lee, A. Guo, V. L. Goss, E. J. Spek, H. Zhang, X. M. Zha, R. D. Polakiewicz, M. J. Comb, Immunoaffinity profiling of tyrosine phosphorylation in cancer cells. *Nat. Biotechnol.* **23**, 94–101 (2005).
26. A. Zimman, S. S. Chen, E. Komisopoulou, B. Titz, R. Martínez-Pinna, A. Kafi, J. A. Berliner, T. G. Graeber, Activation of aortic endothelial cells by oxidized phospholipids: A phosphoproteomic analysis. *J. Proteome Res.* **9**, 2812–2824 (2010).
27. N. P. Shah, C. Tran, F. Y. Lee, P. Chen, D. Norris, C. L. Sawyers, Overriding imatinib resistance with a novel ABL kinase inhibitor. *Science* **305**, 399–401 (2004).
28. M. R. Burgess, B. J. Skaggs, N. P. Shah, F. Y. Lee, C. L. Sawyers, Comparative analysis of two clinically active BCR-ABL kinase inhibitors reveals the role of conformation-specific binding in resistance. *Proc. Natl. Acad. Sci. U.S.A.* **102**, 3395–3400 (2005).
29. G. Q. Daley, D. Baltimore, Transformation of an interleukin 3-dependent hematopoietic cell line by the chronic myelogenous leukemia-specific $P210^{bcr/abl}$ protein. *Proc. Natl. Acad. Sci. U.S.A.* **85**, 9312–9316 (1988).
30. S. Li, R. L. Ilaria Jr., R. P. Million, G. Q. Daley, R. A. Van Etten, The P190, P210, and P230 forms of the *BCR/ABL* oncogene induce a similar chronic myeloid leukemia–like syndrome in mice but have different lymphoid leukemogenic activity. *J. Exp. Med.* **189**, 1399–1412 (1999).
31. T. G. Graeber, J. R. Heath, B. J. Skaggs, M. E. Phelps, F. Remacle, R. D. Levine, Maximal entropy inference of oncogenicity from phosphorylation signaling. *Proc. Natl. Acad. Sci. U.S.A.* **107**, 6112–6117 (2010).
32. J. Y. J. Wang, Antibodies for phosphotyrosine: Analytical and preparative tool for tyrosyl-phosphorylated proteins. *Anal. Biochem.* **172**, 1–7 (1988).
33. T. S. Keshava Prasad, R. Goel, K. Kandasamy, S. Keerthikumar, S. Kumar, S. Mathivanan, D. Telikicherla, R. Raju, B. Shafreen, A. Venugopal, L. Balakrishnan, A. Marimuthu, S. Banerjee, D. S. Somanathan, A. Sebastian, S. Rani, S. Ray, C. J. Harrys Kishore, S. Kanth, M. Ahmed, M. K. Kashyap, R. Mohmood, Y. L. Ramachandra, V. Krishna, B. A. Rahiman, S. Mohan, P. Ranganathan, S. Ramabadran, R. Chaerkady, A. Pandey, Human Protein Reference Database—2009 update. *Nucleic Acids Res.* **37**, D767–D772 (2009).
34. J. C. Obenauer, L. C. Cantley, M. B. Yaffe, Scansite 2.0: Proteome-wide prediction of cell signaling interactions using short sequence motifs. *Nucleic Acids Res.* **31**, 3635–3641 (2003).
35. S. Hunter, R. Apweiler, T. K. Attwood, A. Bairoch, A. Bateman, D. Binns, P. Bork, U. Das, L. Daugherty, L. Duquenne, R. D. Finn, J. Gough, D. Haft, N. Hulo, D. Kahn, E. Kelly, A. Laugraud, I. Letunic, D. Lonsdale, R. Lopez, M. Madera, J. Maslen, C. McAnulla, J. McDowall, J. Mistry, A. Mitchell, N. Mulder, D. Natale, C. Orengo, A. F. Quinn, J. D. Selengut, C. J. Sigrist, M. Thimma, P. D. Thomas, F. Valentin, D. Wilson, C. H. Wu, C. Yeats, InterPro: The integrative protein signature database. *Nucleic Acids Res.* **37**, D211–D215 (2009).
36. Z. Songyang, K. L. Carraway III, M. J. Eck, S. C. Harrison, R. A. Feldman, M. Mohammadi, J. Schlessinger, S. R. Hubbard, D. P. Smith, C. Eng, M. J. Lorenzo, B. A. J. Ponder, B. J. Mayer, L. C. Cantley, Catalytic specificity of protein-tyrosine kinases is critical for selective signalling. *Nature* **373**, 536–539 (1995).
37. M. D. Schaller, Paxillin: A focal adhesion-associated adaptor protein. *Oncogene* **20**, 6459–6472 (2001).
38. P. Van Slyke, M. L. Coll, Z. Master, H. Kim, J. Filmus, D. J. Dumont, Dok-R mediates attenuation of epidermal growth factor-dependent mitogen-activated protein kinase and Akt activation through processive recruitment of c-Src and Csk. *Mol. Cell. Biol.* **25**, 3831–3841 (2005).
39. K. Neet, T. Hunter, The nonreceptor protein-tyrosine kinase CSK complexes directly with the GTPase-activating protein-associated p62 protein in cells expressing v-Src or activated c-Src. *Mol. Cell. Biol.* **15**, 4908–4920 (1995).
40. S. Danhauser-Riedl, M. Warmuth, B. J. Druker, B. Emmerich, M. Hallek, Activation of Src kinases $p53/56^{lyn}$ and $p59^{hck}$ by $p210^{bcr/abl}$ in myeloid cells. *Cancer Res.* **56**, 3589–3596 (1996).
41. W. Lu, D. Gong, D. Bar-Sagi, P. A. Cole, Site-specific incorporation of a phosphotyrosine mimetic reveals a role for tyrosine phosphorylation of SHP-2 in cell signaling. *Mol. Cell* **8**, 759–769 (2001).
42. J. Chen, W. M. Yu, H. Daino, H. E. Broxmeyer, B. J. Druker, C. K. Qu, SHP-2 phosphatase is required for hematopoietic cell transformation by Bcr-Abl. *Blood* **109**, 778–785 (2007).
43. M. Dance, A. Montagner, J. P. Salles, A. Yart, P. Raynal, The molecular functions of Shp2 in the Ras/Mitogen-activated protein kinase (ERK1/2) pathway. *Cell. Signal.* **20**, 453–459 (2008).
44. B. W. Howell, J. A. Cooper, Csk suppression of Src involves movement of Csk to sites of Src activity. *Mol. Cell. Biol.* **14**, 5402–5411 (1994).
45. G. Superti-Furga, S. Fumagalli, M. Koegl, S. A. Courtneidge, G. Draetta, Csk inhibition of c-Src activity requires both the SH2 and SH3 domains of Src. *EMBO J.* **12**, 2625–2634 (1993).
46. M. T. Brown, J. A. Cooper, Regulation, substrates and functions of Src. *Biochim. Biophys. Acta* **1287**, 121–149 (1996).
47. W. Fiskus, M. Pranpat, P. Bali, M. Balasis, S. Kumaraswamy, S. Boyapalle, K. Rocha, J. Wu, F. Giles, P. W. Manley, P. Atadja, K. Bhalla, Combined effects of novel tyrosine kinase inhibitor AMN107 and histone deacetylase inhibitor LBH589 against Bcr-Abl–expressing human leukemia cells. *Blood* **108**, 645–652 (2006).
48. M. Thai, P. Y. Ting, J. McLaughlin, D. Cheng, M. Müschen, O. N. Witte, J. Colicelli, ABL fusion oncogene transformation and inhibitor sensitivity are mediated by the cellular regulator RIN1. *Leukemia* **25**, 290–300 (2011).
49. P. H. Huang, F. M. White, Phosphoproteomics: Unraveling the signaling web. *Mol. Cell* **31**, 777–781 (2008).
50. K. Rikova, A. Guo, Q. Zeng, A. Possemato, J. Yu, H. Haack, J. Nardone, K. Lee, C. Reeves, Y. Li, Y. Hu, Z. Tan, M. Stokes, L. Sullivan, J. Mitchell, R. Wetzel, J. Macneill,

J. M. Ren, J. Yuan, C. E. Bakalarski, J. Villen, J. M. Kornhauser, B. Smith, D. Li, X. Zhou, S. P. Gygi, T. L. Gu, R. D. Polakiewicz, J. Rush, M. J. Comb, Global survey of phosphotyrosine signaling identifies oncogenic kinases in lung cancer. *Cell* **131**, 1190–1203 (2007).
51. P. Filippakopoulos, M. Kofler, O. Hantschel, G. D. Gish, F. Grebien, E. Salah, P. Neudecker, L. E. Kay, B. E. Turk, G. Superti-Furga, T. Pawson, S. Knapp, Structural coupling of SH2-kinase domains links Fes and Abl substrate recognition and kinase activation. *Cell* **134**, 793–803 (2008).
52. R. Linding, L. J. Jensen, G. J. Ostheimer, M. A. van Vugt, C. Jorgensen, I. M. Miron, F. Diella, K. Colwill, L. Taylor, K. Elder, P. Metalnikov, V. Nguyen, A. Pasculescu, J. Jin, J. G. Park, L. D. Samson, J. R. Woodgett, R. B. Russell, P. Bork, M. B. Yaffe, T. Pawson, Systematic discovery of in vivo phosphorylation networks. *Cell* **129**, 1415–1426 (2007).
53. A. Sirvent, C. Bénistant, J. Pannequin, L. Veracini, V. Simon, J. F. Bourgaux, F. Hollande, F. Cruzalegui, S. Roche, Src family tyrosine kinases-driven colon cancer cell invasion is induced by Csk membrane delocalization. *Oncogene* **29**, 1303–1315 (2010).
54. S. Mitra, C. Beach, G. S. Feng, R. Plattner, SHP-2 is a novel target of Abl kinases during cell proliferation. *J. Cell Sci.* **121**, 3335–3346 (2008).
55. J. F. Cloutier, L. M. Chow, A. Veillette, Requirement of the SH3 and SH2 domains for the inhibitory function of tyrosine protein kinase p50csk in T lymphocytes. *Mol. Cell. Biol.* **15**, 5937–5944 (1995).
56. D. Davidson, J. F. Cloutier, A. Gregorieff, A. Veillette, Inhibitory tyrosine protein kinase p50csk is associated with protein-tyrosine phosphatase PTP-PEST in hemopoietic and non-hemopoietic cells. *J. Biol. Chem.* **272**, 23455–23462 (1997).
57. Y. P. Chong, T. D. Mulhern, H. J. Zhu, D. J. Fujita, J. D. Bjorge, J. P. Tantiongco, N. Sotirellis, D. S. S. Lio, G. Scholz, H. C. Cheng, A novel non-catalytic mechanism employed by the C-terminal Src-homologous kinase to inhibit Src-family kinase activity. *J. Biol. Chem.* **279**, 20752–20766 (2004).
58. B. B. Au-Yeung, S. E. Levin, C. Zhang, L. Y. Hsu, D. A. Cheng, N. Killeen, K. M. Shokat, A. Weiss, A genetically selective inhibitor demonstrates a function for the kinase Zap70 in regulatory T cells independent of its catalytic activity. *Nat. Immunol.* **11**, 1085–1092 (2010).
59. G. Sun, A. K. Sharma, R. J. Budde, Autophosphorylation of Src and Yes blocks their inactivation by Csk phosphorylation. *Oncogene* **17**, 1587–1595 (1998).
60. S. Gonfloni, A. Weijland, J. Kretzschmar, G. Superti-Furga, Crosstalk between the catalytic and regulatory domains allows bidirectional regulation of Src. *Nat. Struct. Biol.* **7**, 281–286 (2000).
61. J. Wu, F. Meng, L. Y. Kong, Z. Peng, Y. Ying, W. G. Bornmann, B. G. Darnay, B. Lamothe, H. Sun, M. Talpaz, N. J. Donato, Association between imatinib-resistant *BCR-ABL* mutation-negative leukemia and persistent activation of LYN kinase. *J. Natl. Cancer Inst.* **100**, 926–939 (2008).
62. P. J. Johnson, P. M. Coussens, A. V. Danko, D. Shalloway, Overexpressed pp60$^{c\text{-}src}$ can induce focus formation without complete transformation of NIH 3T3 cells. *Mol. Cell. Biol.* **5**, 1073–1083 (1985).
63. J. Dengjel, V. Akimov, J. V. Olsen, J. Bunkenborg, M. Mann, B. Blagoev, J. S. Andersen, Quantitative proteomic assessment of very early cellular signaling events. *Nat. Biotechnol.* **25**, 566–568 (2007).
64. C. Ritz, J. C. Streibig, Bioassay analysis using R. *J. Stat. Softw.* **12**, 1–22 (2005).
65. J. E. Elias, W. Haas, B. K. Faherty, S. P. Gygi, Comparative evaluation of mass spectrometry platforms used in large-scale proteomics investigations. *Nat. Methods* **2**, 667–675 (2005).
66. S. A. Beausoleil, J. Villen, S. A. Gerber, J. Rush, S. P. Gygi, A probability-based approach for high-throughput protein phosphorylation analysis and site localization. *Nat. Biotechnol.* **24**, 1285–1292 (2006).
67. A. Prakash, P. Mallick, J. Whiteaker, H. Zhang, A. Paulovich, M. Flory, H. Lee, R. Aebersold, B. Schwikowski, Signal maps for mass spectrometry-based comparative proteomics. *Mol. Cell. Proteomics* **5**, 423–432 (2006).
68. M. B. Eisen, P. T. Spellman, P. O. Brown, D. Botstein, Cluster analysis and display of genome-wide expression patterns. *Proc. Natl. Acad. Sci. U.S.A.* **95**, 14863–14868 (1998).
69. S. E. Ong, M. Mann, A practical recipe for stable isotope labeling by amino acids in cell culture (SILAC). *Nat. Protoc.* **1**, 2650–2660 (2006).
70. R. Amanchy, D. E. Kalume, A. Pandey, Stable isotope labeling with amino acids in cell culture (SILAC) for studying dynamics of protein abundance and posttranslational modifications. *Sci. STKE* **2005**, pl2 (2005).
71. A. J. Link, J. Labaer, In-gel trypsin digest of gel-fractionated proteins. *Cold Spring Harb. Protoc.* **2009**, pdb.prot5110 (2009).
72. G. E. Crooks, G. Hon, J. M. Chandonia, S. E. Brenner, WebLogo: A sequence logo generator. *Genome Res.* **14**, 1188–1190 (2004).
73. R. A. Fisher, *Statistical Methods for Research Workers* (Oliver and Boyd, Edinburgh, 1925).
74. Y. Benjamini, Y. Hochberg, Controlling the false discovery rate: A practical and powerful approach to multiple testing. *J. R. Stat. Soc. Ser. B Stat. Methodol.* **57**, 289–300 (1995).
75. A. Subramanian, P. Tamayo, V. K. Mootha, S. Mukherjee, B. L. Ebert, M. A. Gillette, A. Paulovich, S. L. Pomeroy, T. R. Golub, E. S. Lander, J. P. Mesirov, Gene set enrichment analysis: A knowledge-based approach for interpreting genome-wide expression profiles. *Proc. Natl. Acad. Sci. U.S.A.* **102**, 15545–15550 (2005).
76. **Acknowledgments:** We thank H. Herschman [University of California-Los Angeles (UCLA)] for generously providing the pMvsrc plasmid, C. Sawyers (Memorial Sloan-Kettering Cancer Center) for the pMSCVpuro-p210 plasmid, and N. Graham for critical reading of the manuscript. **Funding:** B.T. is a postdoctoral fellow of the German Academic Exchange Service, and S.S.C. is a recipient of the UCLA Tumor Biology Program U.S. Department of Health and Human Services Ruth L. Kirschstein Institutional National Research Service Award # T32 CA009056. M.M. is a scholar of the Leukemia and Lymphoma Society (LLS1497-11) and is supported by NIH grants R01CA137060 and R01CA139032. T.G.G. is an Alfred P. Sloan Research Fellow. Funding for the research was provided by grants to T.G.G. from the NIH NHGRI (HG002807) and the University of California Cancer Research Coordinating Committee. **Author contributions:** L.R., B.T., L.B., E.G., T.L., and M.T. performed the experiments. B.T., E.K., and S.S.C. performed MS analysis. L.R., B.T., E.K., M.P., and T.G.G. performed the data and bioinformatic analyses. B.S. and M.M. provided reagents and interpreted the data. L.R. and T.G.G. wrote the manuscript. **Competing interests:** The authors declare that they have no competing interests. **Data availability:** The MS data associated with this manuscript may be downloaded from http://systems.crump.ucla.edu/data/.

Submitted 29 June 2010
Accepted 1 January 2011
Final Publication 29 March 2011
10.1126/scisignal.2001314
Citation: L. Rubbi, B. Titz, L. Brown, E. Galvan, E. Komisopoulou, S. S. Chen, T. Low, M. Tahmasian, B. Skaggs, M. Müschen, M. Pellegrini, T. G. Graeber, Global phosphoproteomics reveals crosstalk between Bcr-Abl and negative feedback mechanisms controlling Src signaling. *Sci. Signal.* **4**, ra18 (2011).